

Volumetric Radar Echo Motion Estimation Using Physics-Informed Deep Learning: A Case Study Over Slovakia

Peter Pavlík, Anna Bou Ezzeddine, Viera Rozinajová

Abstract—Motion estimation from spatiotemporal Earth observation data is a key component of many forecasting and monitoring systems. In precipitation nowcasting, most extrapolation-based methods rely on two-dimensional radar composites to estimate the horizontal motion of precipitation systems. However, in some cases, precipitation systems can exhibit varying motion at different heights. We propose a physics-informed convolutional neural network that estimates independent horizontal motion fields for multiple altitude layers directly from volumetric radar reflectivity data and investigate the practical benefits of altitude-wise motion field estimation for precipitation nowcasting. The model is trained end-to-end on volumetric observations from the Slovak radar network and its extrapolation nowcasting performance is evaluated. We compare the proposed model against an architecturally identical baseline operating on vertically pooled two-dimensional radar composites. Our results show that, although the model successfully learns altitude-wise motion fields, the estimated displacement is highly correlated across vertical levels for the vast majority of precipitation events. Consequently, the volumetric approach does not yield systematic improvements in nowcasting accuracy. While categorical metrics indicate increased precipitation detection at longer lead times, this gain is largely attributable to non-physical artifacts and is accompanied by a growing positive bias. A comprehensive inter-altitude motion field correlation analysis further confirms that events exhibiting meaningful vertical variability in horizontal motion are rare in the studied region. We conclude that, for the Slovak radar dataset, the additional complexity of three-dimensional motion field estimation is not justified by questionable gains in predictive skill. Nonetheless, the proposed framework remains applicable in climates where precipitation systems exhibit stronger vertical variability in horizontal motion.

Index Terms—Weather Radar, Nowcasting, Neural networks

I. INTRODUCTION

PRECIPITATION nowcasting refers to the task of predicting the intensity and spatial distribution of precipitation (rain, snow, hail, etc.) over the next few hours with high local accuracy [1]. These short-term forecasts are crucial for early warning systems, helping to reduce damage and save lives during extreme weather events. As the climate crisis drives greater variability in precipitation patterns [2], improving nowcasting capabilities is becoming key in making the world’s societies and economies more resilient.

Precipitation nowcasting typically relies on observations from ground-based weather radars, which estimate the location

and intensity of hydrometeors within their coverage area. In its simplest form, nowcasting is performed by examining a sequence of past radar images, inferring the recent motion – its direction and speed – and then extrapolating the latest observation forward in time. This principle forms the foundation of traditional optical-flow-based approaches, which, despite their simplicity, can still outperform numerical weather prediction (NWP) models at lead times of up to a few hours [3].

To compensate for the limitations of simple radar extrapolation, traditional nowcasting systems typically include an additional post-processing step that estimates the evolution of precipitation – its growth, decay, and structural changes. Historically, statistical or heuristic approaches have been leveraged to adjust the extrapolated radar fields according to the trends in recent observations. Examples of traditional algorithms that also predict growth and decay to some extent using statistical methods are S-PROG [4] with its extensions STEPS [5] and LINDA [6]; or ANVIL [7].

In recent years, deep learning models have transformed the landscape of precipitation nowcasting. Early works like ConvLSTM [8], PredRNN [9], or RainNet [10], treat nowcasting as a direct sequence-to-sequence prediction problem, taking several past radar frames as input and generating future fields. These models often outperformed classical statistical post-processing, but they struggled to fully capture the physical mechanisms governing precipitation without explicit modeling of the displacement due to advection.

When machine learning-based models are trained to minimize traditional gridpoint-based loss functions, the chaotic nature of the atmosphere gives rise to the so-called double penalty problem: a forecast that accurately captures the intensity, size, and timing of a precipitation feature but not the advection displacement is penalized twice – once for missing the event at the true location and once for predicting it at the wrong one [11]. As a result, models tend to produce mathematically optimal predictions that appear overly smooth and blurry, lacking physical realism. This smoothing effect particularly degrades the representation of extreme events, which are dampened or smeared out, thereby limiting the practical value of such forecasts for early warning applications.

More recent deep learning models explicitly incorporate motion modeling into their architectures. Models such as TrajGRU [12], DGMR [13], NowcastNet [14], or L-CNN [15] introduce learned motion fields or motion-aware components that separate the tasks of advection and precipitation field evolution. This hybrid paradigm that combines explicit movement

Peter Pavlík is a PhD student at the Faculty of Information Technology, Brno University of Technology, Czechia.

All authors are members of the Green and Secure Environment group at the Kempten Institute of Intelligent Technologies (KInIT) in Bratislava, Slovakia.

modeling with deep learning-based estimation of growth and decay has led to major improvements in spatial accuracy at longer lead times, mitigating the blurring effect of the double penalty problem [16].

While deep learning has significantly advanced precipitation nowcasting, most existing approaches operate on two-dimensional radar composites and therefore assume that precipitation advection can be sufficiently represented in a vertically collapsed space. This assumption simplifies the problem and is totally adequate in many cases, but it neglects the three-dimensional structure of atmospheric motion, where vertical wind shear and inter-altitude flow differences may influence the horizontal displacement of precipitation features.

Some prior studies have explored the use of three-dimensional radar observations for precipitation nowcasting. Three-dimensional convolutional neural networks have been applied to volumetric radar data and demonstrated improvements in forecast skill, suggesting that vertical structure and height-dependent motion can provide additional predictive information [17]–[19]. In addition to fully data-driven approaches, three-dimensional optical flow methods have also been investigated for nowcasting in some regions [19], [20]. More recently, the Nowcast3D model successfully employed a novel deep learning architecture to estimate volumetric motion fields from radar data, reporting improved performance across a range of evaluation scenarios, outperforming baseline approaches [21]. However, the extent to which explicitly modeled volumetric motion fields contribute to nowcasting performance, independent of other architectural choices, remains unclear.

In this work, we train a deep learning model to estimate volumetric motion fields from sequences of radar reflectivity volumes and use these fields to extrapolate the precipitation forward in time separately at each altitude. We examine whether explicitly modeling three-dimensional precipitation advection offers practical advantages for precipitation nowcasting using a dataset from 4 radar stations in Slovakia. To focus specifically on the role of advection, we intentionally exclude precipitation growth and decay processes from the forecast, allowing for a more controlled investigation and comparison between two- and three-dimensional motion representations. Thanks to the fast inference of the deep learning model, we can perform a robust evaluation of the whole dataset and present the quantitative as well as qualitative results.

II. OPTICAL FLOW AND NOWCASTING

Most traditional precipitation nowcasting methods are based on the assumption of persistence – that precipitation in the near future will closely resemble the present state. In an Eulerian framework, this assumption corresponds to simply repeating the most recent observation, accuracy of which quickly drops with increasing lead time as precipitation systems move.

A more realistic formulation adopts a Lagrangian perspective, in which precipitation features are assumed to persist while being transported by an advection (motion) field. Under this view, nowcasting is reduced to estimating a motion field and advecting the most recent precipitation observation forward in time according to this field. This assumption forms the

basis of classical radar extrapolation and optical-flow-based nowcasting methods. Under this view, the temporal evolution of the precipitation field is governed by the advection equation:

$$\frac{\partial \Psi}{\partial t} + \nabla \cdot (\Psi \mathbf{u}) = 0 \quad (1)$$

where Ψ denotes the 2D radar precipitation field and \mathbf{u} the horizontal motion field. For simplification, it is commonly assumed that the flow is incompressible, i.e., $\nabla \cdot \mathbf{u} = 0$.

The right side in this formulation expresses the Lagrangian persistence assumption – the change in precipitation intensity along flow trajectories defined by the motion field \mathbf{u} is zero. Traditional radar extrapolation and optical-flow-based nowcasting methods rely directly on this assumption by estimating \mathbf{u} from recent observations and advecting the most recent precipitation field forward in time.

In practice, the quality of such Lagrangian nowcasts depends heavily on the accuracy of the estimated motion field. Classical methods typically infer the motion field \mathbf{u} from sequences of 2D radar images using optical flow techniques such as the Lucas-Kanade algorithm [22], assuming that precipitation motion can be adequately represented in two dimensions.

An example of an optical flow approach taking into account the full 3D extent of the radar data is provided in [20], where the spatiotemporal characteristics of motion fields derived from three-dimensional radar echoes over Taiwan were investigated. In their work, the motion field is still defined purely in the horizontal plane, but is estimated independently for each altitude level using volumetric radar reflectivity, thereby allowing the horizontal advection to vary with height while neglecting explicit vertical velocity components. Their analysis shows that this height-resolved formulation can be beneficial in situations characterized by strong vertical variability of echo motion, particularly during deep convective events, Meiyu front (eastward mesoscale convective system), and typhoons interacting with complex terrain. In these scenarios, significant differences in motion speed and direction were observed between lower and upper levels, leading to reduced inter-altitude correlation and improved representation of echo advection compared to two-dimensional composite-based motion fields. Conversely, the authors report that in stratiform precipitation with limited vertical echo extent, motion fields remain highly correlated across heights, limiting the practical benefit of the volumetric approach.

Moving beyond the altitude-wise separation of horizontal motion, recent deep learning frameworks have attempted to directly model the full three-dimensional evolution of weather systems by coupling physical operators with data-driven representations. A prominent example is the Nowcast3D [21] model, which treats radar reflectivity evolution not merely as advection, but as a composite of three physical processes: three-dimensional advection, local diffusion, and a source term representing microphysical tendencies. Unlike the independent altitude-wise estimation in [20], Nowcast3D reconstructs a complete 3D velocity field, including the vertical component, directly from volumetric reflectivity. This deterministic core is further refined by a conditional diffusion module designed

to capture stochastic uncertainty. While the authors report superior performance over operational baselines in forecasting extreme convective events, such as the 2024 Beijing heavy rainfall, they also acknowledge inherent ambiguity in the approach. As the authors note, the inference of a full 3D motion field solely from reflectivity observations remains an under-constrained problem, particularly in regimes dominated by complex microphysics where phase changes alter reflectivity without corresponding changes in velocity.

Section II Summary

Classical optical-flow-based nowcasting methods rely on the Lagrangian persistence assumption, whereby precipitation features are passively advected by an estimated horizontal motion field. While extensions of this framework to volumetric radar data allow horizontal advection to vary with height, existing studies indicate that such height-resolved motion fields are only beneficial under specific conditions, notably in deep convective systems, strongly sheared environments, and require dense radar coverage. In contrast, stratiform precipitation with limited vertical echo extent tends to exhibit highly correlated motion across altitudes, reducing the practical advantage of volumetric motion estimation.

More recent deep learning approaches attempt to move beyond pure advection by directly modeling the three-dimensional evolution of radar echoes. However, these methods highlight a fundamental challenge shared with motion-based approaches: inferring dynamical structure solely from reflectivity observations is inherently under-constrained and sensitive to data quality, particularly in regimes dominated by complex microphysical processes. Together, these considerations suggest that modeling volumetric flow does not universally translate into improved nowcasting performance, motivating a careful evaluation of when volumetric motion modeling is warranted.

III. VOLUMETRIC RADAR DATA

Ground weather radar stations provide three-dimensional observations of precipitation systems by repeatedly scanning the atmosphere at multiple elevation (sweep) angles. Each volume scan consists of a sequence of conical sweeps at increasing elevation angles, which together sample radar reflectivity across a range of heights above the surface. By combining these individual sweeps, a volumetric representation of the precipitation field can be constructed, capturing the vertical structure of reflectivity that is closely linked to microphysical processes, storm intensity, and precipitation evolution.

While the native radar measurements are collected in polar coordinates, these multi-angle observations can be interpolated onto a Cartesian grid to form three-dimensional radar volumes suitable for quantitative analysis and data-driven modeling.

Many operational nowcasting systems rely on two-dimensional products such as column-maximum reflectivity (CMAX) or constant-altitude plan position indicators (CAPPI).

However, volumetric radar data offers additional information about the vertical extent and structure of precipitation echoes that cannot be recovered from 2D composites alone.

A. Slovak Climate Conditions

The experiments in this study are based on volumetric radar reflectivity data from the Slovak national weather radar network consisting of 4 ground radar stations. They provide three-dimensional scans of precipitation at multiple elevation angles and at temporal resolutions suitable for nowcasting applications. Climatological analysis of thunderstorm occurrences in Slovakia from 1984–2023 documents a pronounced seasonal cycle with peak activity in June and July, spatial variability related to topography, and typical frequencies of 16 thunderstorm days per year, consistent with a continental, mid-latitude convective regime [23]. While deep convective storms occur episodically during the warm season, particularly under conditions of strong surface heating and instability, they represent a smaller fraction of precipitation events compared to large-scale stratiform systems.

Based on the prevailing meteorological conditions in the Slovak region, certain characteristics of the vertical reflectivity structure are to be anticipated. Stratiform precipitation systems – generally typified by feeble vertical motions, low precipitation intensity and considerable spatial uniformity [24] – are most common, whereas convective precipitation systems – typically connected to intense vertical motions, high precipitation intensity, and pronounced spatial variability [24] – are more localized and occurring primarily during the warm season. From a nowcasting perspective, such deep convective precipitation events represent scenarios in which altitude-wise motion estimation could provide valuable additional information beyond two-dimensional composites. These expectations motivate a systematic evaluation of volumetric motion fields across different conditions, including time of year, in the subsequent sections.

B. The Radar Dataset

The radar dataset we use consists of volumetric radar reflectivity data collected from the Slovak national weather radar network – four C-band Doppler radar stations located at Malý Javorník, Kojšovská hoľa, Kubínska hoľa, and Španí laz (see Fig. 1). The radar network provides volumetric scans at 5-minute intervals, enabling the analysis of precipitation evolution at temporal resolutions suitable for short-term nowcasting.

The dataset spans the period of four years from 12 June 2018 to 22 August 2022 and contains observations from select events with significant radar echo measurements. The selected events are approximately uniformly distributed throughout the year, covering a wide range of meteorological conditions (see Table. I). Radar observations were mapped to a Cartesian grid with a horizontal resolution of 1 km \times 1 km, resulting in images of size 517 \times 755 pixels. Vertically, each radar volume spans 16 altitude levels ranging from 500 m to 8000 m above ground level, capturing both low-level precipitation structures and deeper storm development.

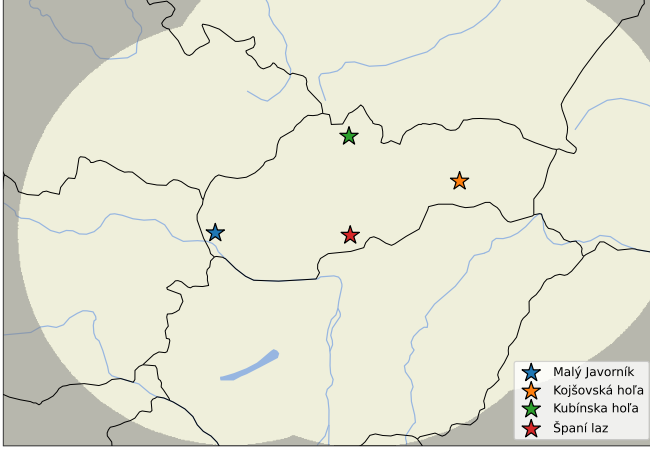


Fig. 1. The figure shows the locations of the four ground radar stations comprising the Slovak radar network. The overlapping lightly shaded circular areas show the maximum extent of the radar coverage.

TABLE I
MONTHLY DISTRIBUTION OF RADAR VOLUME OBSERVATIONS IN THE DATASET.

Month	Obs. (No.)	Obs. (%)
January	2858	10.30
February	1724	6.21
March	1698	6.12
April	2867	10.33
May	2581	9.30
June	1723	6.21
July	2866	10.33
August	2290	8.25
September	2276	8.20
October	2574	9.28
November	2003	7.22
December	2290	8.25
Total	27750	100.00

Radar measurements are provided in terms of equivalent reflectivity factor (dBZ). For model training and evaluation, reflectivity values were converted to precipitation intensity expressed in mm h^{-1} using the Marshall-Palmer Z-R reflectivity-rain rate relationship [25]. This presents a more physically interpretable learning target useful both for model training and evaluation.

Parts of the selected grid fall outside the effective observation range of one or more radars (see Fig. 1). In addition, the radar stations do not have continuous uptime over the entire study period. As summarized in Table II, three of the four stations achieve high data availability exceeding 96%, while the Španí laz radar exhibits substantially lower uptime, being unavailable for almost one third of the selected observation times. Despite these limitations, the central portion of the domain is consistently well covered by multiple radars, with more than 96% of all radar volumes consisting of data captured by three or more radars operating simultaneously (see Table III).

To reduce storage requirements and speed up the data loading and processing, radar-derived precipitation fields were quantized to 8-bit precision prior to further analysis. This quantization preserves the precipitation patterns relevant for

TABLE II
RADAR DATA AVAILABILITY (UPTIME) FOR EACH STATION OVER THE STUDY PERIOD.

Radar station	Missing (No.)	Available (No.)	Uptime (%)
Malý Javorník	733	27017	97.36
Kojšovská hoľa	946	26804	96.59
Kubínska hoľa	1032	26718	96.28
Španí laz	8107	19643	70.79

TABLE III
DISTRIBUTION OF RADAR VOLUME OBSERVATIONS BY THE NUMBER OF SIMULTANEOUSLY AVAILABLE RADAR STATIONS.

Active radars	Observations (No.)	Observations (%)
4	18565	66.90
3	8127	29.29
2	483	1.74
1	575	2.07
Total	27750	100.00

motion estimation while significantly reducing data volume.

C. Preprocessing and Quality Control

Radar reflectivity measurements are inherently affected by various sources of noise and uncertainty, including non-meteorological echoes, beam geometry effects, and intermittent data gaps. Such artifacts can significantly degrade motion estimation and disrupt the training of machine learning-based nowcasting methods. Consequently, appropriate preprocessing and denoising are essential to ensure that the input data represents physically meaningful precipitation structures.

In the volumetric dataset, non-meteorological echoes and small-scale noise were suppressed using a combination of polarimetric filtering and morphological operations applied to the radar reflectivity fields. First, the copolar correlation coefficient (ρ_{HV}) was used to identify non-meteorological targets. Reflectivity values at grid points with $\rho_{HV} < 0.6$ were removed, as such low correlation values are associated with clutter, biological scatterers, or other non-precipitating returns.

Following polarimetric filtering, additional spatial denoising was performed using morphological opening operations applied independently to each altitude level. First, a binary mask identifying non-zero reflectivity regions was constructed. This mask was then subjected to repeated binary opening using a diamond-shaped structuring element, removing small, isolated echo regions while preserving larger coherent precipitation structures. To prevent erosion of small-but-intense convective cores, regions with reflectivity exceeding 40 dBZ were identified and expanded using binary dilation, and were exempted from removal during the opening process. Grid points identified as noise by the opening operation and not belonging to high reflectivity regions were subsequently set to zero. The comparison between the raw observation and the result of the denoising process is shown in Figure 2.

All morphological operations were applied in the horizontal plane only, ensuring that denoising did not introduce artificial vertical correlations between altitude levels.

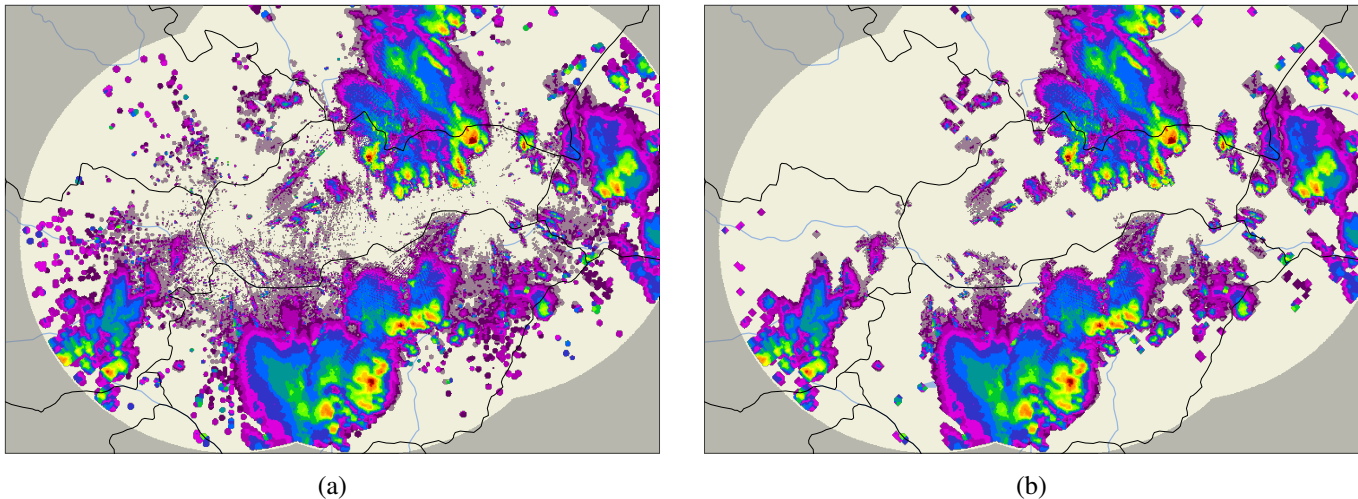


Fig. 2. Example of the radar reflectivity denoising process: (a) raw reflectivity field containing non-meteorological echoes and small-scale noise, and (b) corresponding reflectivity field after polarimetric filtering and morphological denoising. Both of the images are created by displaying the vertical column maximum from the 3D volume for each pixel (CMAX).

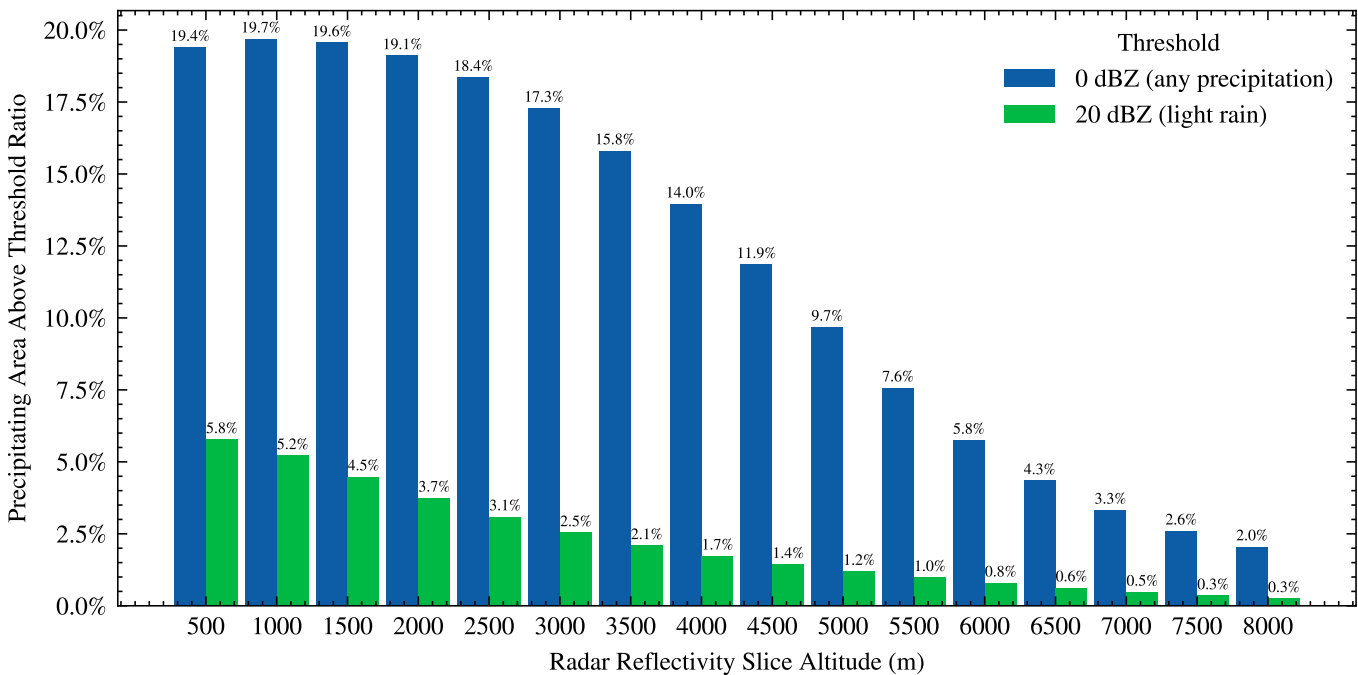


Fig. 3. Bar chart showing the mean fraction of grid points with reflectivity exceeding 0 and 20 dBZ at each altitude level. A rapid decrease in rainy pixel occurrence with height is observed, reflecting the limited vertical extent of many precipitation events in the dataset.

D. Preliminary Data Analysis

To learn more about the vertical structure of precipitation in the dataset, we first perform a descriptive analysis of the denoised volumetric radar observations. In particular, we examine how frequently precipitation echoes exhibit substantial vertical extent across multiple altitude levels, as opposed to being confined to a shallow layer near the surface. To this end, we compute, for each radar volume sample, the fraction of grid points exceeding specified reflectivity thresholds at each altitude level. These fractions are evaluated using two reflectivity thresholds: 0 dBZ to quantify the overall occurrence of any precipitation echoes and 20 dBZ to represent light rain and

above. See the calculated ratios in Figure 3.

At the lower reflectivity threshold representing the occurrence of any precipitation echoes, the mean fraction of rainy pixels decreases from nearly 20 % at 1 km above ground level to approximately 2 % at 8 km. A similar trend is observed at the higher threshold, where the fraction of pixels exceeding 20 dBZ declines from about 6 % near the surface to roughly 0.3 % at the highest altitude level. These results indicate that the majority of precipitation events in the dataset exhibit limited vertical development, with only a small subset displaying appreciable reflectivity at upper altitudes. This does not present a promising outlook for the utility of volumetric

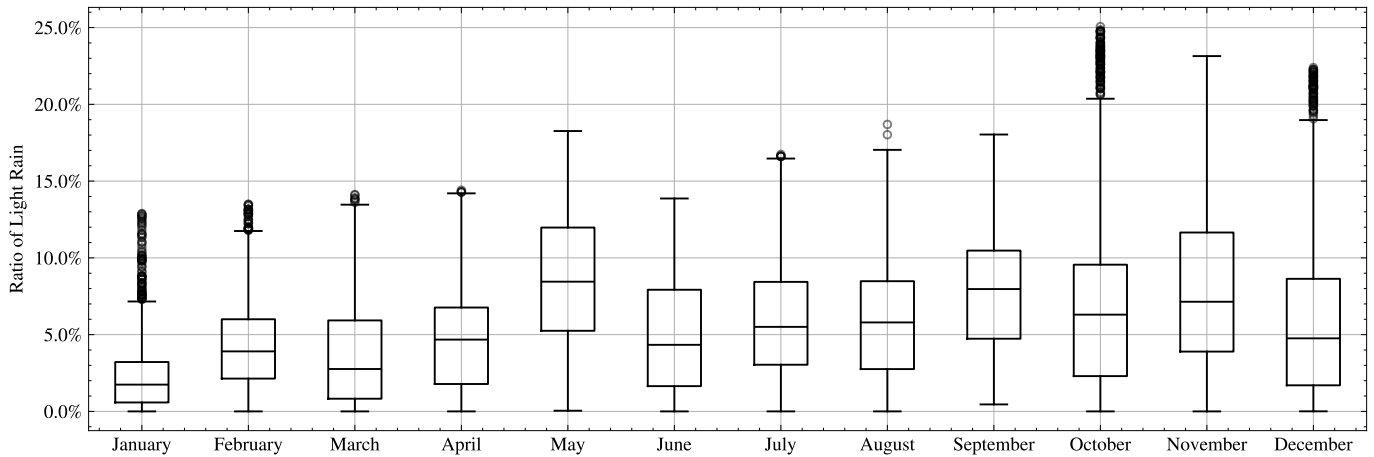


Fig. 4. Month-wise distribution of rainy pixel ratios in the dataset. For each radar volume, the ratio of light precipitation was computed as the percentage of pixels exceeding 20 dBZ at the lowest altitude slice (500 m above ground level). Boxes span the interquartile range (Q1–Q3), with the median indicated by a horizontal line. Whiskers extend to the most extreme values within 1.5 times the interquartile range, while points beyond the whiskers denote outliers.

motion fields in the general case.

Additionally, to illustrate the variability of overall event intensity in the dataset, we construct month-wise boxplots of rainy pixel ratios at the lowest altitude level (500 m above ground level). For each radar volume, the ratio is computed as the percentage of pixels exceeding a reflectivity threshold of 20 dBZ, and the resulting distributions are shown in Fig. 4. The rainy pixel ratios appear to be relatively evenly distributed across the year, although the first third of the year exhibits lower median values. Since convective precipitation events, which predominantly occur during the summer months, are expected to benefit most from altitude-resolved motion estimation, this seasonal imbalance is not expected to negatively impact the subsequent analysis.

We further explore the potential benefit of volumetric data by analyzing the degree of similarity between precipitation structures observed at different altitude levels, specifically for the samples with meaningful echoes at higher altitudes. Even if in most cases the vertical extent of precipitation is not high, cases where such behavior is present might still benefit a lot. We expect that strongly correlated reflectivity patterns across heights are likely to give rise to similar motion estimates, thereby reducing the potential benefit of estimating independent motion fields for each layer. On the other hand, if low correlation across altitudes is observed, the utility of volumetric motion fields is likely worth the effort. To quantify this relationship, we compute the Pearson correlation coefficient between all pairs of altitude-specific reflectivity volume slices. Pearson correlation of reflectivity emphasizes spatial pattern similarity and not intensity magnitude, which makes it fit for data meant for motion estimation. Correlations are evaluated using a subset of radar volumes in which non-zero reflectivity is present at all altitude levels. Out of a total of 25358 radar volume samples, 5621 satisfy this criterion. The resulting correlation matrix is shown in Fig. 5.

The resulting correlation matrix reveals a high degree of vertical coherence in radar reflectivity structures across the majority of altitude levels. Strong correlations are observed

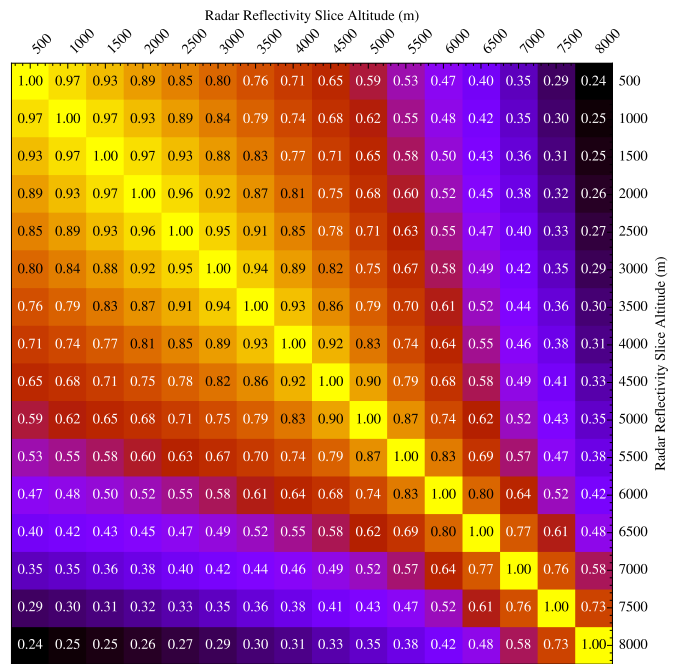


Fig. 5. Correlation matrix showing the mean pixel-wise Pearson correlation coefficients between horizontally co-located radar reflectivity slices at different altitude levels from 500 to 8000 m above ground level. Only samples where non-zero reflectivity was observed at each altitude were included in the calculation.

not only between adjacent layers, but also across several kilometers of vertical separation, with correlation coefficients decreasing smoothly with increasing height difference. Even within this subset of precipitation events with high vertical extent, reflectivity patterns remain strongly aligned between lower and mid-levels, and only gradually decorrelate toward the highest altitudes. This behavior indicates that precipitation structures in the examined dataset are predominantly vertically coherent, exhibiting limited horizontal displacement between altitude levels. From the perspective of motion estimation, such strong vertical correlation implies that separate reflectiv-

ity slices provide largely redundant information for inferring horizontal advection. Consequently, the potential benefit of estimating independent motion fields for each altitude layer is expected to be limited in the general case, as similar spatial patterns across heights are likely to produce highly similar motion estimates. However, volumetric motion estimation might still prove beneficial for a subset of events with lower inter-altitude correlation and should be investigated.

Section III Summary

We presented and described the volumetric radar reflectivity dataset, along with the used data denoising scheme, and performed the preliminary data analysis. Unfortunately, majority of data samples show only limited vertical extent and even the samples with significant vertical extent show a high level of vertical coherence.

Despite the strong vertical coherence observed in the majority of samples, the volumetric motion estimation may still offer benefits under specific conditions. For this reason, we proceed with a systematic evaluation of volumetric motion field estimation, with the aim of identifying scenarios in which height-resolved advection provides measurable improvements over two-dimensional approaches.

IV. 3D MOTION FIELD U-NET

In this section, we introduce the deep learning model developed for estimating precipitation motion fields from volumetric radar data as well as the utilized training objective and optimization procedure. The model is designed to predict altitude-wise horizontal motion fields from three-dimensional radar volumes, enabling an explicit investigation of height-dependent advection in line with classical radar extrapolation methods.

A. Initial Architecture Exploration

Before selecting a final architecture for evaluating the utility of multi-altitude motion fields, we explored several design choices for processing the four-dimensional spatiotemporal radar data (three spatial dimensions and time). As we intended to use a 3D U-Net architecture, consisting of standard three-dimensional convolutional layers available in all deep learning libraries, it is necessary to determine which dimensions are explicitly represented spatially and which are encoded along the channel dimension.

A natural formulation suggests representing the three spatial dimensions – longitude, latitude, and altitude – as a volumetric input, with the temporal dimension encoded as channels. While this representation is intuitive, prior work in precipitation nowcasting has shown that explicitly modeling time as a separate dimension, rather than collapsing it into the channel axis, can lead to improved performance [26]–[28]. This observation motivated an initial exploration of architectural configurations that differ in how spatial and temporal dimensions are represented.

After dissatisfactory results of multiple architectures trained to produce a full 3D motion field in a single forward pass,

we opted to emulate the approach employed in [20], where horizontal motion fields were computed independently for each two-dimensional horizontal slice of the volumetric radar volume sequence. The model predicts a single time-invariant motion field per slice, intended to represent the dominant horizontal advection governing near-future precipitation evolution. The horizontal slicing not only simplifies the task, but has a few benefits:

- Possibility of treating time as a third dimension, enabling more effective spatiotemporal feature extraction and improving the performance of the model, without requiring 4D convolutional neural layers.
- An identical neural network architecture can be used both for the 2D CMAX benchmark model and for the volumetric case (applied iteratively to each altitude slice), ensuring a fair and controlled comparison between 2D and volumetric motion estimation.
- Improved interpretability, as motion fields and the accordingly extrapolated reflectivity fields can be directly analyzed and compared across individual altitude levels without interference from vertical mixing.

The horizontal slicing approach also entails certain limitations. First, vertical motion components, which may be relevant during intense convective events, are not explicitly modeled. However, in preliminary experiments involving full three-dimensional motion fields with an explicit vertical component, the model failed to learn stable or physically meaningful vertical motion, and required strong constraints to converge. Removing the vertical motion component resulted in more stable training and improved overall performance.

Second, interactions between neighboring altitude levels cannot directly influence the estimated motion at a given height. Since the analysis in Section III-D indicates strong correlations between reflectivity fields at adjacent altitudes, explicitly enforcing vertical coupling may be unnecessary and would further homogenize the estimated motion fields, suppressing subtle differences in motion across different altitudes. Independent motion estimation for individual layers should emphasize subtle inter-layer differences where they exist.

In summary, we adopt an approach in which the volumetric radar observations are decomposed into a set of two-dimensional horizontal altitude slices, and a separate horizontal-only motion field is estimated for each slice using a 3D U-Net architecture with time treated as an explicit third dimension. The resulting altitude-wise horizontal motion fields are subsequently stacked to produce a pseudo-3D motion field without an explicit vertical velocity component.

B. 3D Motion Field Estimation Network

To process sequences of consecutive radar reflectivity slices, we employ a 3D U-Net neural network. The model is a fully convolutional architecture closely related to the standard and widely used U-Net, with the key difference that all two-dimensional convolutional layers are replaced by three-dimensional convolutions. This modification allows the network to operate on constant-altitude reflectivity slices stacked

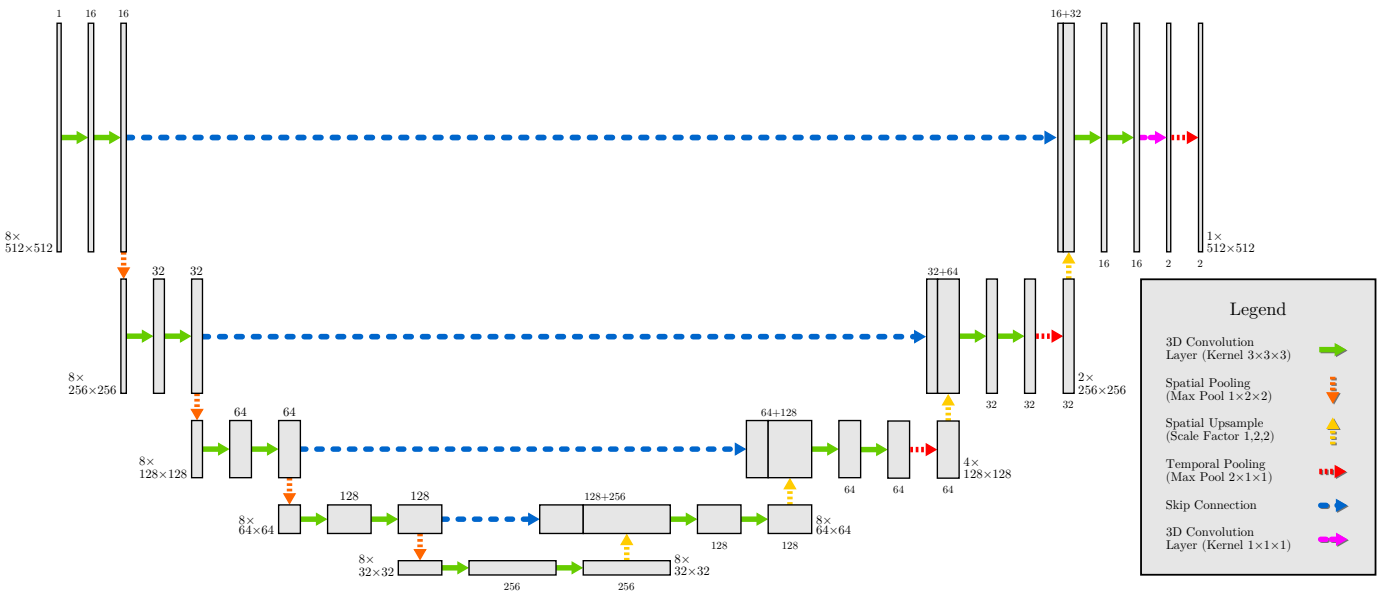


Fig. 6. The figure illustrates the 3D U-Net architecture used for horizontal motion field estimation. Feature map blocks indicate tensor dimensions, with the first dimension representing time and the remaining two corresponding to horizontal spatial coordinates. The encoder progressively reduces spatial resolution while increasing channel depth using 3D convolutions and spatial pooling, whereas the decoder restores resolution via upsampling and reduces the number of channels by convolutional processing. Skip connections link corresponding encoder and decoder stages to preserve fine-scale spatial information. The temporal dimension is gradually collapsed in the decoder, yielding a single motion field representing the dominant advection over the input (and near-future) radar sequence. The final layer outputs two channels corresponding to the horizontal motion components.

along the temporal dimension, treating them as a unified spatiotemporal input volume.

By explicitly modeling time as an additional dimension rather than as independent channels, the network can learn temporally coherent features and motion patterns, which has been shown to improve performance in precipitation nowcasting tasks.

With this configuration, the model processes each horizontal slice of the volumetric radar data independently. Consequently, estimating the volumetric motion field for a single radar volume would require 16 sequential forward passes, assuming 16 vertical levels are used. To avoid this inefficiency, we modify the model’s data loading and inference pipeline to treat each altitude slice as an independent sample and process all slices of a volume jointly as a batch. This batching strategy is used solely for computational efficiency and does not introduce information exchange between altitude levels during inference. The resulting slice-wise motion fields are then stacked along the vertical dimension to form a pseudo-3D motion field.

We now describe the model architecture in more detail (see Fig. 6 for a schematic overview). The network receives as input a stacked sequence of radar images corresponding to a fixed altitude level, which together form a single-channel three-dimensional spatiotemporal volume with dimensions corresponding to longitude, latitude, and time.

The 3D U-Net architecture follows an encoder–decoder design with skip connections between corresponding resolution levels. In the encoder, the spatial resolution in the horizontal dimensions (longitude and latitude) is progressively reduced through pooling operations, while the number of feature channels is increased to capture increasingly abstract spatiotemporal representations. The temporal dimension is

preserved throughout the encoder, allowing the encoder to reason about motion cues present across consecutive time steps at each layer.

At the bottleneck, the encoded representation is passed to the decoder, which mirrors the encoder by progressively restoring the horizontal spatial resolution while reducing the number of feature channels. Skip connections transfer high-resolution spatial features from the encoder to the decoder, facilitating precise localization of motion structures. In the decoder, the temporal dimension is gradually aggregated and collapsed, such that the final output has a temporal extent of one.

Collapsing the temporal dimension at the output is necessary as the objective of the network is to infer a single, time-invariant horizontal motion field that captures the displacement of precipitation features across the input sequence and into the near future.

The final output has two channels corresponding to the horizontal components of the estimated motion field.

C. Training the 3D Motion Field U-Net

Training a neural network to estimate physically meaningful horizontal advection fields \mathbf{u} for precipitation extrapolation is a non-trivial task. To be effective within a volumetric Lagrangian persistence framework, the estimated motion field must represent a temporally consistent horizontal displacement pattern that explains the evolution of precipitation features across the observed sequence, while remaining spatially smooth and free of spurious sources or sinks.

The simplest training strategy would minimize the discrepancy between a single extrapolated precipitation field and its immediate successor at the next time step. Denoting by

$\xi^1(\Psi_t, \mathbf{u})$ the precipitation field Ψ_t advected forward by one time step using motion field \mathbf{u} , such a loss can be written as:

$$\mathcal{L}_{\text{single}} = \mathcal{C}\left(\xi^1(\Psi_t, \mathbf{u}), \hat{\Psi}_{t+1}\right), \quad (2)$$

where \mathcal{C} is an error criterion and $\hat{\Psi}_{t+1}$ denotes the ground-truth observation.

In practice, this simple formulation leads to motion fields that overly adapt to individual frame transitions and exhibit unrealistic local divergence and convergence patterns. While such fields may reduce short-term extrapolation error, they fail to capture a coherent advection structure representative of the entire observed sequence.

To address these limitations, we introduce two key modifications to the training procedure.

1) *Sequence-consistent motion estimation*: Rather than optimizing the motion field using a single input–target pair, we require a single estimated motion field to explain the temporal evolution of precipitation across an extended sequence consisting of both past observations and future ground-truth fields. Specifically, given an input sequence of n observed precipitation fields $\{\Psi_1, \dots, \Psi_n\}$ and a set of m subsequent future observations $\{\hat{\Psi}_{n+1}, \dots, \hat{\Psi}_{n+m}\}$, which are not available to the model at inference time, we minimize the extrapolation error across all consecutive pairs in the concatenated sequence:

$$\mathcal{L}_{\text{MF}} = \sum_{t=1}^{n+m-1} \mathcal{C}\left(\xi^1(\Phi_t, \mathbf{u}), \Phi_{t+1}\right), \quad (3)$$

where $\Phi = \{\Psi_1, \dots, \Psi_n, \hat{\Psi}_{n+1}, \dots, \hat{\Psi}_{n+m}\}$ denotes the combined sequence.

By optimizing the motion field to remain valid across both observed and future frames, the model is encouraged to infer an advection pattern that is stable and predictive over the nowcasting horizon, rather than one that merely explains short-term transitions within the input sequence.

2) *Multi-scale pooling*: To further stabilize training and discourage the encoding of small-scale noise into the motion field, the extrapolation loss is evaluated across multiple spatial scales. Both precipitation fields and the estimated motion field are average-pooled using increasing kernel sizes, with the motion vectors rescaled accordingly to preserve physical consistency. The total data-driven loss is obtained by averaging extrapolation errors across all pooling levels, biasing the model toward coherent large-scale motion patterns while retaining sensitivity to finer structures when supported by the data.

3) *Physics-informed regularization*: In addition to the data-driven extrapolation loss, we incorporate a physics-informed regularization term that penalizes violations of the incompressibility assumption and conservation of mass. Specifically, we discourage divergence in the estimated horizontal motion field by penalizing the magnitude of its divergence:

$$\nabla \cdot \mathbf{u} = \frac{\partial u_x}{\partial x} + \frac{\partial u_y}{\partial y} \quad (4)$$

Spatial derivatives are approximated using discrete convolutions with 3×3 Sobel filters. The resulting regularization term to be minimized is defined as:

$$\mathcal{L}_{\text{PI}} = |\nabla \cdot \mathbf{u}| \quad (5)$$

This term acts as a soft physical constraint, guiding the network toward motion fields that are more consistent with the continuity equation while allowing deviations where supported by the data.

4) *Final loss function*: The overall objective minimized during training is a weighted combination of the data-driven and physics-informed terms:

$$\mathcal{L} = (1 - \beta) \mathcal{L}_{\text{MF}} + \beta \mathcal{L}_{\text{PI}}, \quad \beta \in (0, 1) \quad (6)$$

This formulation balances accurate sequence-wide precipitation extrapolation with physically plausible motion estimation and was found to produce stable and accurate motion fields.

D. Data Preprocessing and Input Construction

Prior to training, the radar observations undergo a series of preprocessing steps designed to ensure physical consistency, numerical stability, and computational efficiency, while preserving the information relevant for motion estimation.

1) *Temporal sampling and sequence construction*: Each training sample consists of a sequence of 8 consecutive input time steps, corresponding to 40 minutes of observations given the 5-minute temporal resolution of the radar data. To encourage the estimation of motion fields that remain predictive beyond the immediate future, the training loss additionally incorporates 16 subsequent future observations, spanning a total forecasting horizon of 80 minutes. These future frames are used exclusively for loss computation and are not provided to the model as inputs.

2) *Reflectivity-to-rain-rate conversion and normalization*: The raw radar reflectivity observations are first converted from reflectivity space to rain rate using the Marshall–Palmer relationship [25], converting them from logarithmic reflectivity (dBZ) to units of rain rate (mm h^{-1}).

To stabilize training and reduce the dynamic range of the inputs, we apply a logarithmic dBR normalization to the rain-rate fields. Specifically, rain-rate values above a small threshold are transformed as

$$\text{dBR} \mapsto 10 \log_{10}(R), \quad (7)$$

while values below the threshold are mapped to a fixed minimum value of -15 . This transformation preserves the ordering of precipitation intensities while preventing numerical issues arising from extremely small or zero rain-rate values.

3) *Noise removal and quality control*: All radar volumes are denoised prior to normalization using the polarimetric and morphological filtering procedure described in Section III-C. This step removes non-meteorological echoes and isolated noise artifacts, ensuring that the motion estimation network is trained on physically meaningful precipitation structures.

4) *Spatial cropping and data augmentation*: During training, random 512×512 spatial crops are extracted from the full radar volumes. This ensures that the input resolution matches the model requirement of being divisible by 16, while the random crop positions increase the diversity of spatial configurations encountered during training. To further improve generalization, the data are augmented using random horizontal and vertical flips.

Grid points falling outside the effective observation range of the radar network are masked and excluded from loss computation. This ensures that the optimization is driven solely by regions with valid radar observations and prevents the model from learning spurious motion patterns in areas with missing or unobserved data.

5) *Vertical resolution reduction*: Although the original radar volumes contain 16 vertical levels spanning altitudes from 500 m to 8000 m above ground level, we reduce the vertical resolution to 8 levels for model training. This is achieved by max-pooling adjacent altitude pairs (e.g., 500–1000 m, 1000–1500 m, etc.).

This design choice represents a deliberate compromise between computational complexity and informational content. As shown by the correlation analysis in Section III-D, reflectivity fields at neighboring altitudes are strongly correlated, indicating substantial redundancy across vertical levels. Pooling adjacent layers therefore preserves the dominant precipitation structures while substantially reducing computational cost.

An additional benefit of the pooling is that information is not completely discarded: max-pooling retains the strongest reflectivity signal within each altitude pair. This design enables a fair comparison with the CMAX baseline, as subsequent pooling of all vertical levels into a single composite field corresponds directly to the CMAX representation because the operation is associative.

Section IV Summary

This section details the 3D U-Net architecture and the training methodology employed to estimate altitude-resolved horizontal motion fields. By decomposing radar volumes into individual horizontal slices and treating time as an explicit third dimension, the model captures spatiotemporal features more effectively than channel-collapsed approaches. The training process utilizes a multi-scale sequence-consistent loss function that optimizes the motion field across both observed and future frames, reinforced by a physics-informed divergence penalty to ensure the estimated advection physically plausible. To balance computational efficiency with meteorological detail, the vertical resolution is reduced from 16 to 8 levels via max-pooling, which preserves the most intense reflectivity structures while minimizing vertical redundancy.

V. EVALUATION

In this section, we evaluate the performance of the proposed volumetric motion field estimation framework for precipitation nowcasting based on Lagrangian persistence assumption and then analyze the properties of the resulting motion fields in detail.

First, in Section V-A, we assess the effectiveness of volumetric motion estimation by establishing a controlled baseline. An identical 3D U-Net architecture is trained on two-dimensional CMAX inputs and compared against the volumetric model.

Subsequently, we turn to an analysis of the estimated volumetric motion fields themselves. In Section V-B, we quantify the similarity of motion estimates across altitude levels by computing correlation matrices of the derived motion fields. By examining these correlations both globally and month-wise, we investigate potential seasonal dependencies and identify meteorological situations in which low vertical coherence may indicate added value from volumetric motion estimation. Finally, we present a qualitative analysis of selected precipitation events to highlight cases where three-dimensional advection should provide the most benefit based on inter-level correlation and precipitation coverage.

A. Nowcasting Performance of 2D vs. 3D Extrapolation

To assess the added value of volumetric motion field estimation, we train an architecturally identical baseline – 3D Motion Field U-Net – to produce a 2D motion field and compare its nowcasting performance against the proposed model that produces a volumetric motion field. The two models are virtually identical in structure and training procedure, differing only in the form of the input data: either radar observations pooled into a single CMAX image or represented by eight stacked altitude-wise slices spanning the radar volume. This design ensures that any observed performance differences can be attributed solely to the use of volumetric information rather than architectural or optimization-related factors. Both models are trained and validated using data up to January 1, 2022 (approximately 3.5 years), with all subsequent observations reserved exclusively for nowcasting performance evaluation (approximately 8 months).

Nowcasting performance is evaluated by simply advecting the final input observation forward in time using the estimated motion field under the Lagrangian persistence assumption – with no increase or decrease in precipitation intensity over time. To ensure a fair and controlled comparison, the forecasts produced by the volumetric model are subsequently collapsed into two-dimensional CMAX representations prior to evaluation. This allows us to directly determine whether altitude-resolved advection provides a measurable advantage over the standard two-dimensional baseline.

Predictive performance is quantified using a combination of continuous and categorical verification metrics. Mean Error (ME) is used to assess systematic bias, while Mean Absolute Error (MAE) and Mean Squared Error (MSE) quantify overall forecast accuracy. We also compute precision, recall, and the Equitable Threat Score (ETS) over binarized precipitation maps at precipitation intensity thresholds of 1, 5, and 10 mm h^{-1} , corresponding to light, moderate, and heavy precipitation regimes. All metrics are computed independently for each forecast lead time across the 80-minute nowcasting horizon.

1) *Quantitative Results*: We begin the quantitative evaluation by comparing the Mean Absolute Error (MAE) and Mean Squared Error (MSE) of the baseline model trained on pooled CMAX radar observations with those of the proposed volumetric motion field model. These two metrics typically exhibit similar behavior, with MSE placing greater emphasis

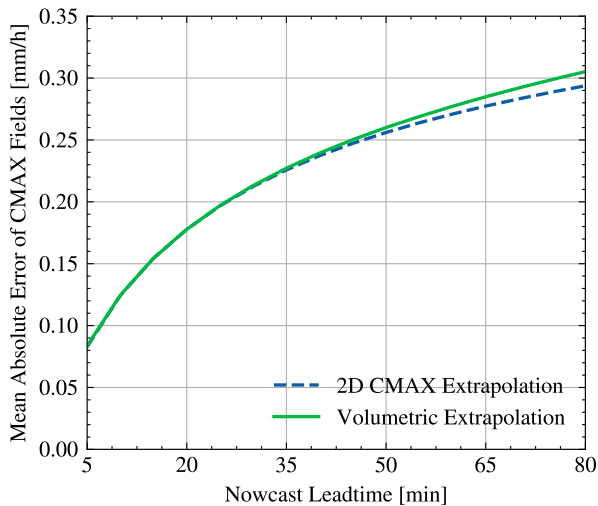


Fig. 7. Mean absolute error of extrapolation-based nowcasts as a function of lead time. The blue dashed line corresponds to the 2D motion field model, while the solid green line represents the volumetric motion field model operating on altitude-wise radar slices.

on large errors. Both MAE and MSE are also affected by the double-penalty problem, whereby spatial displacement errors can lead to higher scores for more visually plausible forecasts. While these metrics alone are insufficient for a definitive assessment of nowcasting skill, they remain useful for analyzing how forecast accuracy degrades with increasing lead time.

We first examine the MAE. Figure 7 shows that both models perform nearly identically up to approximately 30 minutes lead time. Beyond this point, the error curves begin to diverge, with the volumetric model exhibiting a slightly higher MAE at longer lead times.

A similar pattern is observed for the MSE. As shown in Figure 8, both models achieve comparable performance up to roughly 30 minutes lead time, after which the volumetric model again shows marginally higher error.

We next consider the Mean Error (ME), which provides insight into systematic bias of the models. Figure 9 shows that both models exhibit a slight underestimation bias at short lead times. The 2D CMAX-based model maintains a relatively stable bias that gradually approaches zero as lead time increases. In contrast, the volumetric model transitions more rapidly toward a positive bias, indicating increasing overestimation at longer lead times.

From the continuous metrics presented so far, the volumetric model appears to underperform the standard 2D extrapolation baseline, with errors diverging at longer lead times and a progressively increasing positive bias. However, as noted earlier, both MAE and MSE are strongly affected by the double-penalty problem, whereby spatial displacement errors are penalized twice – once at the true location and once at the predicted location.

To obtain a more insightful assessment of the models' ability to correctly predict the evolution of precipitation patterns, we therefore turn to categorical verification metrics computed from thresholded extrapolation forecasts. These metrics

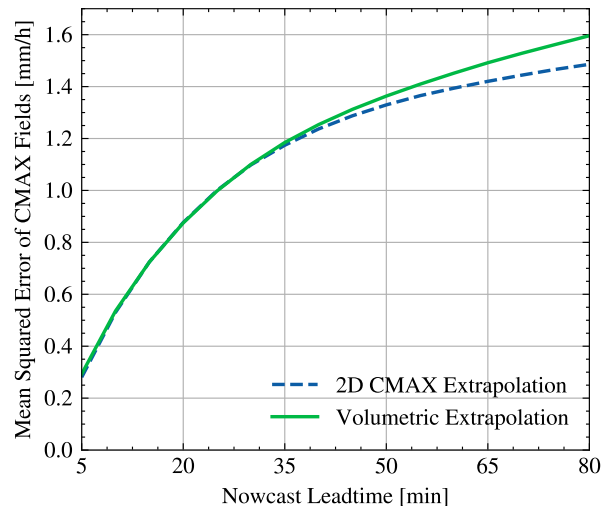


Fig. 8. Mean squared error of extrapolation-based nowcasts as a function of lead time. The blue dashed line corresponds to the 2D motion field model, while the solid green line represents the volumetric motion field model operating on altitude-wise radar slices.

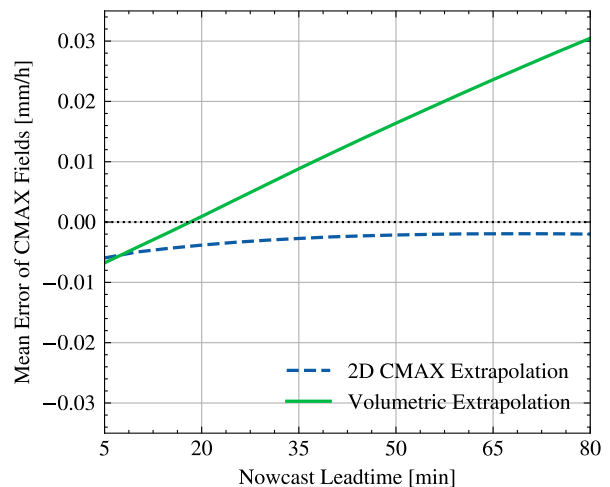


Fig. 9. Mean error (bias) of extrapolation-based nowcasts as a function of lead time. The blue dashed line corresponds to the 2D motion field model, while the solid green line represents the volumetric motion field model operating on altitude-wise radar slices. The black dotted line indicates zero bias.

evaluate the correspondence between predicted and observed precipitation occurrence at different intensity levels, and are less sensitive to spatial misalignments.

We consider three commonly used categorical metrics: Precision, Recall, and the Equitable Threat Score (ETS), evaluated at precipitation intensity thresholds of 1, 5, and 10 mm h^{-1} . For a given threshold, predicted and observed fields are binarized and compared on a pixel-by-pixel basis. Precision measures the fraction of predicted precipitation pixels that are correct, thereby representing the inverse of the false-alarm rate (FAR). Recall measures the fraction of observed precipitation pixels that are successfully detected, reflecting the model's ability to capture existing precipitation.

In precipitation nowcasting, greater emphasis is often placed on Recall – the fraction of observed precipitation events

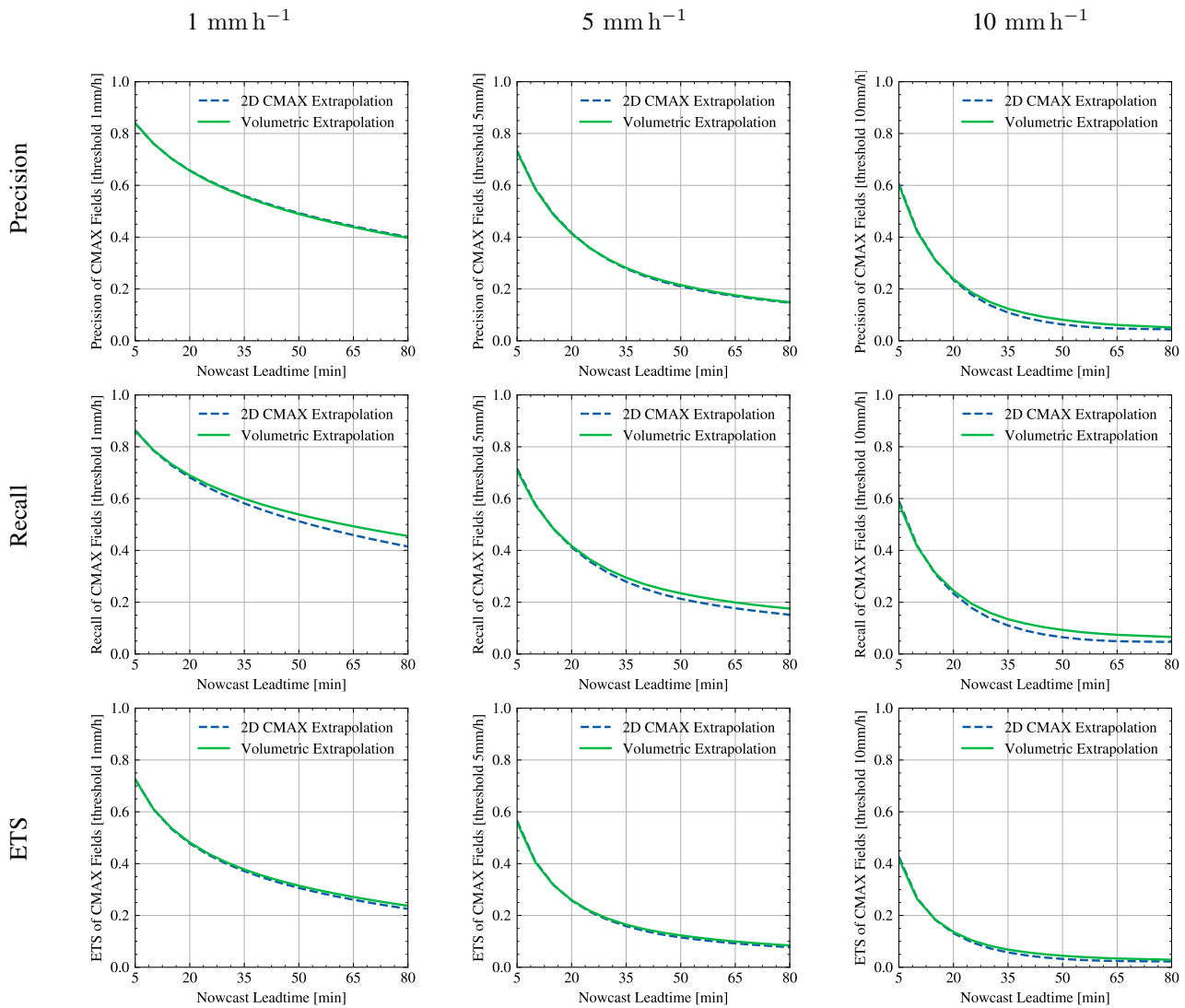


Fig. 10. The figure shows categorical verification metrics – Precision, Recall, and Equitable Threat Score (ETS) – as functions of forecast lead time for the baseline 2D motion-field extrapolation model and the proposed volumetric extrapolation model. Results are shown for precipitation intensity thresholds of 1, 5, and 10 mm h⁻¹. Columns correspond to a fixed binarization threshold, while rows compare the two models using the same metric across the selected thresholds.

that are correctly detected – as high Recall supports timely warnings and hazard awareness. However, this cannot come at the expense of substantially reduced Precision, since excessive false alarms would undermine the practical value of the forecasts. The Equitable Threat Score (ETS) combines information from both Precision and Recall while explicitly accounting for hits that would occur by random chance, making it a widely used metric for nowcasting evaluation.

All the metrics range between 0 and 1, where 0 indicates no skill and 1 corresponds to a perfect nowcast. For each precipitation threshold (1, 5, and 10 mm h⁻¹), the evolution of Precision, Recall, and ETS as a function of forecast lead time is shown in Figure 10.

The categorical metrics reveal a contrasting behavior, with the volumetric model consistently matching or outperforming the baseline 2D approach. The most pronounced differences are observed in Recall, where the volumetric model clearly surpasses the baseline beyond approximately 30 minutes of

lead time across all precipitation thresholds. Importantly, this gain in Recall does not come at the expense of Precision. In fact, Precision is marginally higher for the volumetric model at the highest intensity threshold. The Equitable Threat Score likewise exhibits a small but systematic improvement with increasing lead time at all intensity thresholds, indicating a modest but consistent gain in overall forecast skill.

From an operational nowcasting perspective, the observed improvements in categorical skill are particularly relevant. The enhanced Recall at longer lead times indicates that the volumetric model is more effective at detecting precipitation that will occur in the near future, which is critical for early warning and decision support applications. Importantly, this increase in detection capability is not accompanied by a substantial degradation in Precision, suggesting that the model does not introduce an excessive number of false alarms. The resulting improvement in ETS further confirms that the gain in skill is not incidental but reflects a more informative

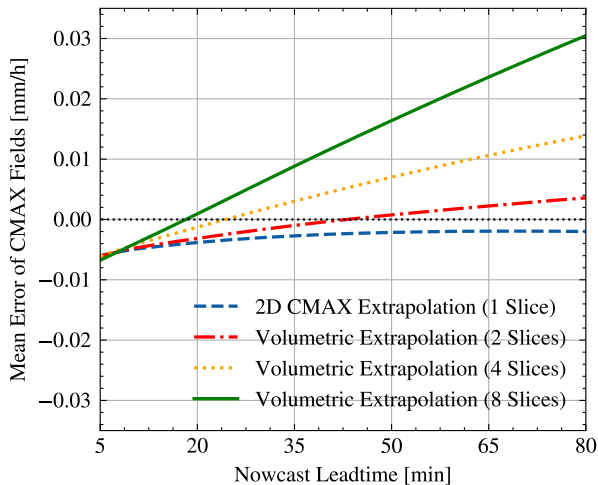


Fig. 11. Mean error (bias) of extrapolation-based nowcasts as a function of lead time. In addition to the baseline 2D CMAX model and the 8-level volumetric model shown in Fig. 9, we include intermediate configurations operating on data pooled to 2 and 4 vertical levels. The black dotted line indicates zero bias.

and reliable forecast. Together, these findings suggest that while volumetric motion estimation may not reduce pixel-wise intensity errors, it can provide meaningful benefits in terms of binary event detection, especially at lead times beyond 30 minutes. However, the observed increase in Recall, together with the growing positive bias at longer lead times, suggests that the volumetric model may exhibit a systematic tendency toward overestimation as the forecast horizon increases.

To investigate the origin of this behavior, we train two additional volumetric motion field models: one operating on radar volumes pooled to four altitude levels and another using only two altitude levels. These models form intermediate configurations between the baseline approach, which operates on data pooled into a single altitude level (i.e., a 2D CMAX slice), and the proposed volumetric model utilizing eight altitude levels. All models are trained using the same architecture, preprocessing, and optimization procedure.

We compare the mean error (bias) of the resulting extrapolation-based nowcasts to assess whether the observed overestimation originates from the model architecture itself and is progressively amplified as the number of independently estimated vertical motion fields increases. The resulting bias curves are shown in Fig. 11.

The results reveal a clear and systematic trend within the volumetric models: as the number of altitude levels increases, the forecasts exhibit progressively stronger overestimation at longer lead times. Although the magnitude of the bias remains relatively small, its consistent growth across configurations suggests that the effect is structural rather than incidental. This behavior therefore warrants further investigation. In the following section, we conduct a qualitative analysis of a selected extreme precipitation event to better understand the underlying cause of this bias.

2) *Qualitative Evaluation*: To complement the quantitative evaluation, we perform a qualitative analysis of a single severe precipitation event from the test set. The selected event corre-

sponds to the most intense volumetric radar observation in the test period by overall reflectivity magnitude and spatial extent. Focusing on such an extreme event allows us to examine the behavior of the proposed volumetric motion field estimator where nowcasting performance is most needed.

The event follows an extended period of extreme heat which was abruptly replaced by a strong convective outbreak associated with a cold front. Severe thunderstorms developed along across western Slovakia. The storms were accompanied by intense rainfall and strong wind gusts with reports of whirlwinds, indicating the presence of organized convective structures and strong low-level shear. Such conditions are expected to produce vertical variability in precipitation fields, making it a natural test case for evaluating the potential benefits of altitude-wise motion estimation. By analyzing the extrapolated volumetric nowcast for this case, we aim to both look for examples of benefits of the volumetric approach and the sources of the systematic bias identified in the quantitative evaluation.

The format constraints of a journal publication limit the direct visualization of volumetric data. We therefore present the results using vertically pooled CMAX representations, while interpreting the observed artifacts in the context of the full three-dimensional radar volumes. Figure 12 shows an 80-minute nowcast of the selected event.

While the magnitudes of the estimated motion fields differ across altitude levels, their orientations are largely consistent at corresponding spatial locations. As a result, the independently estimated motion fields operate as intended, but the benefit of altitude-wise motion estimation in this particular case is limited.

The zoomed-in regions reveal a likely explanation for the increasing positive bias observed at longer lead times. When tracking the northward motion of a single precipitation cell, the model accurately captures the overall displacement and the position of the cell center. However, at the 80-minute lead time, the nowcast exhibits a splitting of the cell into two smaller trailing structures. This artifact arises from slight discrepancies between motion fields estimated at different altitude levels: higher-altitude layers advect more slowly than lower layers, which manifests as apparent cell splitting when the volume is collapsed into a CMAX representation. The corresponding ground-truth observation, by contrast, shows a single coherent cell that has grown in size.

The artificial cell-splitting increases the spatial extent of the predicted precipitation field and contributes to a growing positive bias over time. While such behavior can lead to higher Recall by increasing the area of detected precipitation and largely explains its improvement observed in Section V-A, it does not reflect physically realistic storm evolution. The artifact is a direct consequence of estimating motion fields at different altitude levels fully independently, combined with the evaluation on vertically pooled products. Although the volumetric approach can yield gains in certain metrics, this behavior highlights a key limitation of the current formulation and motivates future work on introducing physically informed vertical consistency into motion field estimation.

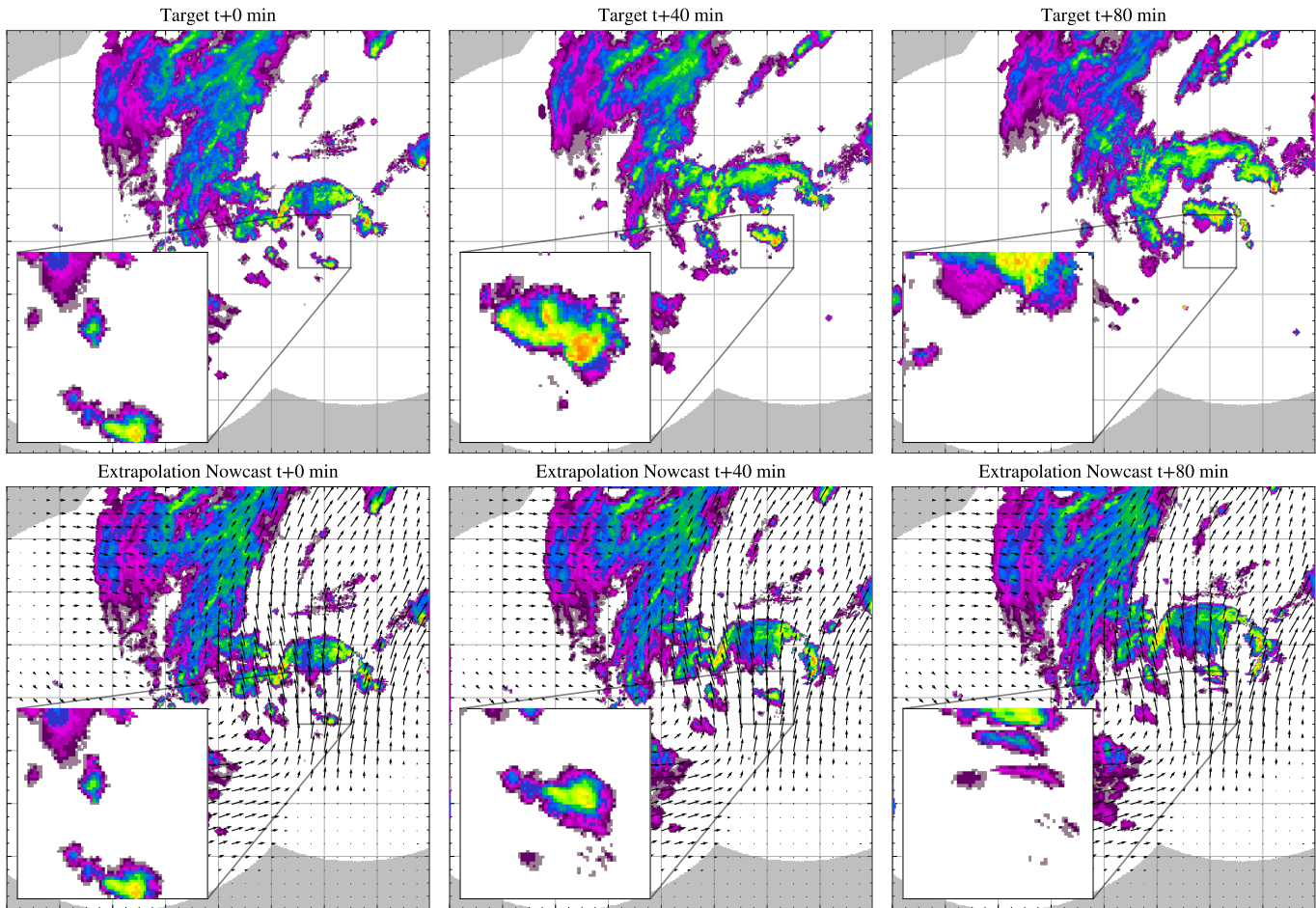


Fig. 12. Vertically pooled CMAX representations of a severe precipitation event over Slovakia on July 5th 2022. The top row shows three consecutive radar observations, with the first image (t+0 min) corresponding to 15:15 UTC and the following two images taken at 40-minute intervals. The bottom row shows the corresponding extrapolations obtained by advecting the final observation using the volumetric motion field estimated by the proposed 3D Motion Field U-Net. The vertically averaged 3D motion field is overlaid for reference. Zoomed regions highlight a non-physical cell-splitting artifact produced by the volumetric approach. The animated figure is available online at: <https://pavlikp.github.io/3DMF/#figure-12>

B. Motion Field Correlation Analysis

Although the proposed volumetric motion field estimator did not yield a clear improvement in overall nowcasting performance, the estimated three-dimensional motion fields remain informative in their own right. The qualitative and quantitative analyses indicate that the model captures mostly physically plausible advection patterns, suggesting that altitude-resolved motion information may still be valuable under specific conditions.

In this subsection, we therefore shift focus from aggregate nowcasting skill to an analysis of the patterns in the estimated volumetric motion fields. In particular, we investigate the degree of similarity between motion fields at different altitude levels by computing inter-layer correlations across the dataset. Strong correlations would indicate largely redundant vertical motion information, while weaker correlations may point to situations where altitude-dependent advection could provide added value.

To this end, motion fields are computed for all available samples, including both training and test data. Unlike the nowcasting evaluation in Section V-A, generalization per-

formance is not a concern. Instead, the goal is to analyze the characteristics of the estimated volumetric motion fields themselves on a per-sample basis. Using training samples is therefore acceptable, as the analysis focuses not on predictive performance but rather on the physical structure and variability of the estimated motion fields.

Based on the correlation analysis, we subsequently identify samples exhibiting unusually low inter-layer correlation, which are hypothesized to have the highest potential benefit from volumetric motion estimation. These cases are then examined qualitatively to assess whether altitude-dependent motion helps to better capture future behavior.

1) *Quantitative Evaluation:* To assess the degree of vertical coherence in the estimated volumetric motion fields, we analyze the similarity between motion fields inferred at different altitude levels. The underlying motivation is that, if altitude-resolved motion estimation is to provide additional value beyond two-dimensional composites, the resulting motion fields should exhibit meaningful vertical variability rather than being near-identical across heights.

For this purpose, we compute pairwise Pearson correlation

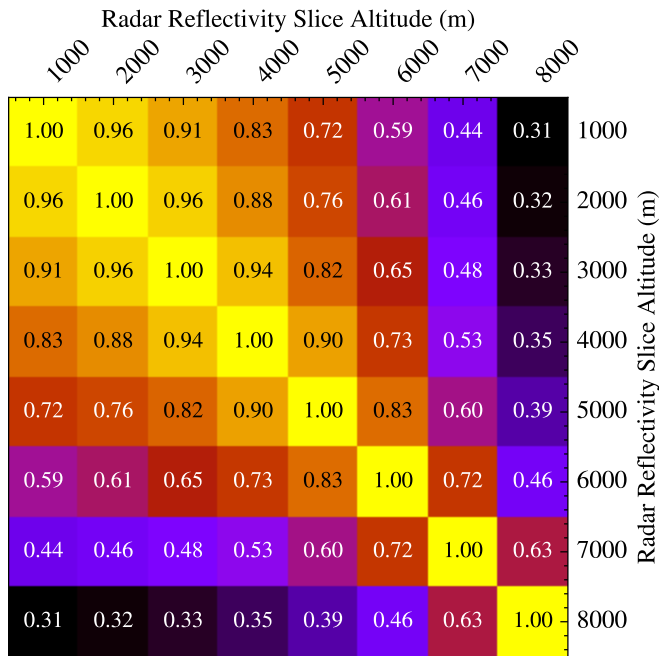


Fig. 13. Mean Pearson correlation coefficients between horizontal motion fields estimated at different altitude levels. Correlations are computed only over precipitating regions and averaged over the full dataset. Note: Each horizontal layer consists of a max-pooled pair of neighboring radar volume slices (altitude 1000 m represents pooled layers at 500 and 1000 m and so on).

coefficients between horizontal motion fields estimated at different altitude levels. The Pearson correlation coefficient quantifies the linear relationship between two fields and provides an interpretable measure of similarity, with values close to one indicating nearly identical motion patterns and values closer to zero suggesting weak correspondence.

Correlations are computed independently for all pairs of altitude levels and averaged over the entire dataset. Importantly, the computation is restricted to spatial regions where precipitation is present. Specifically, for each pair of altitude levels, a binary mask is constructed by taking the sum reflectivity of the corresponding input slice pair and excluding the pixels outside precipitating regions. This prevents large precipitation-free areas from affecting correlation values and ensures that the analysis focuses on relevant regions only.

Figure 13 summarizes the resulting mean correlation matrix for the model operating on 8 vertical levels. Adjacent altitude layers exhibit very strong correlations, typically exceeding 0.9, while correlations decrease gradually with increasing vertical separation. However, even for the most distant altitude pairs, correlations remain moderately strong, with values above 0.3.

Overall, the results indicate that the estimated motion fields are highly vertically coherent. While a gradual decorrelation with altitude distance is present, the magnitude of this effect is limited, suggesting that the dominant horizontal advection patterns are largely shared across vertical levels for most precipitation events in the dataset.

These findings explain the limited performance gains observed in the volumetric nowcasting experiments. Although altitude-resolved motion estimation can capture vertical differ-

ences, such differences appear to be insufficiently pronounced or frequent to yield a consistent improvement over two-dimensional motion estimation when evaluated on aggregate metrics.

Month-wise Motion Correlation: To better understand under which conditions altitude-wise motion estimation may provide added value, we analyze the inter-layer Pearson correlation between the lowest motion field slice (500–1000 m above ground level) and a mid-level slice (2500–3000 m above ground level). The mean correlation between these two layers over the full dataset is very strong – 0.91 (see Fig. 13). These altitude levels were selected based on the precipitation coverage analysis in Fig. 3, as both exhibit comparable rainy pixel ratios while being separated by approximately 1500 m vertically, providing a meaningful vertical contrast. Figure 14 presents the month-wise distribution of inter-layer motion field correlations.

Contrary to our initial hypothesis, the summer months – characterized by a higher prevalence of convective storms – exhibit the highest median correlations and the smallest interquartile ranges. In other words, during periods when deep convection is most common, horizontal motion fields between low and mid-level altitudes tend to be highly coherent. This finding challenges the assumption that warm-season convection would systematically introduce strong vertical differences in horizontal advection. By contrast, several cold-season months display slightly lower median correlations and increased variability.

Overall, these results suggest that vertically distinct horizontal motion patterns are less frequent during convective periods than originally anticipated. To further investigate this behavior, we next examine individual cases exhibiting comparatively low inter-layer correlation. Previous studies, such as [20], have documented events with substantial discrepancies between motion fields at 1.5 and 3 km above ground level. We therefore explore whether similar cases are present in our dataset and assess whether such situations offer tangible benefits for altitude-wise motion estimation.

2) Qualitative Evaluation: For the final qualitative evaluation, we focus on identifying samples that combine high overall precipitation coverage with low inter-altitude motion field correlation. Such cases are most likely to exhibit meaningful differences in horizontal advection between altitude levels, rather than differences arising from noise or weak precipitation signals. As such, they represent the most promising scenarios for assessing whether altitude-resolved motion estimation can capture physically relevant behavior beyond two-dimensional composites.

To identify candidate outliers, we visualize the full dataset using a two-dimensional density histogram that jointly represents (i) the spatial extent of precipitation and (ii) the degree of vertical coherence in the estimated motion fields. Precipitation coverage is quantified as the ratio of CMAX-pooled pixels exceeding a reflectivity threshold of 20 dBZ, while vertical coherence is again measured by the Pearson correlation between motion fields at the lowest (500–1000 m above ground level) and mid-level (2500–3000 m above ground level) altitude slices.

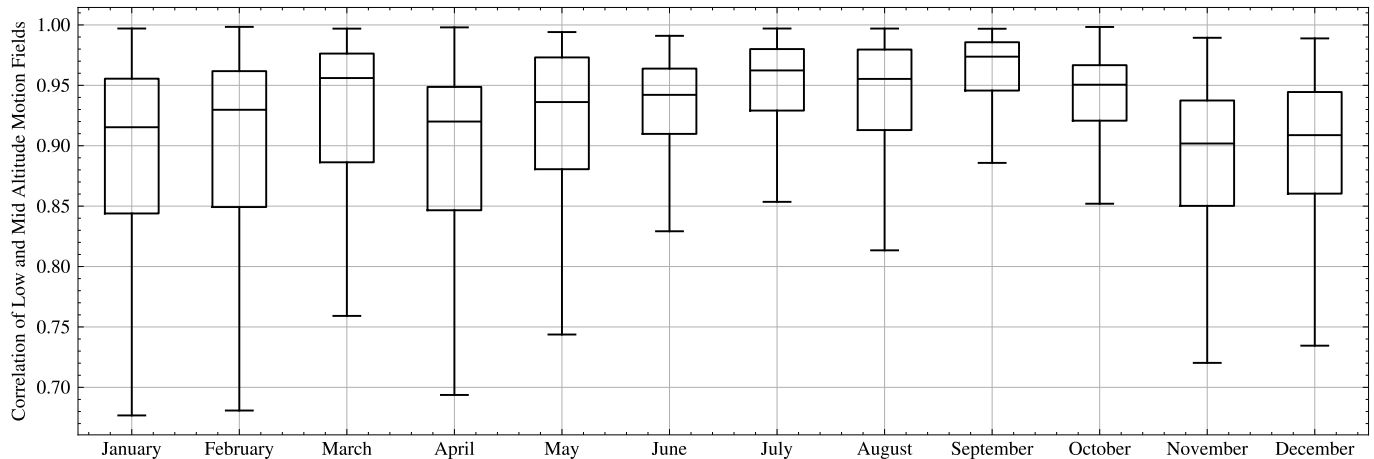


Fig. 14. Month-wise boxplots of Pearson correlation coefficients between horizontal motion fields estimated at the lowest altitude layer (500–1000 m above ground level) and a mid-level layer (2500–3000 m above ground level). Each box represents the interquartile range (Q1–Q3), with the median indicated by a horizontal line. Whiskers extend to the most extreme values within 1.5 times the interquartile range. Outliers are omitted to improve visual clarity and facilitate comparison across months.

The resulting distribution is shown in Figure 15. Regions with high precipitation coverage and low inter-altitude correlation are sparsely populated, indicating that such situations are very rare in the dataset. From this space, we select three representative samples, marked by crosses in the figure, for detailed qualitative inspection of the estimated volumetric motion fields.

The three outlier events were identified using a joint ranking procedure designed to prioritize samples with both extensive precipitation coverage and low inter-altitude motion field correlation. Specifically, all samples were ranked in descending order by precipitation coverage ratio and in ascending order by low-to-mid altitude motion field correlation. The two ranks were then summed to obtain a combined score reflecting overall relevance for qualitative inspection. From this list, the top three events were selected, excluding temporally adjacent samples originating from the same meteorological event.

For each selected case, we visualize the estimated horizontal motion fields at the lowest altitude slice (500–1000 m above ground level) and at the mid-level slice (2500–3000 m above ground level), together with the corresponding precipitation fields. The results are shown in Figure 16.

Across all three cases, the estimated motion fields at the low and mid altitudes appear highly similar at first glance. The most noticeable discrepancy occurs in the lower-left portion of event (a), where the motion transitions from predominantly eastward at low altitude to a more north-easterly direction at mid-levels. However, closer inspection of the precipitation fields and their evolution suggests that this region is affected by ground clutter or partial radar occlusion, leading to unreliable motion estimates rather than physically meaningful vertical shear.

For the remaining cases, even such localized discrepancies are not apparent, and the motion fields remain strongly aligned across altitude levels in terms of motion direction, with some small deviations in magnitude in certain areas – again, mostly data-sparse areas like the circles directly above the ground

radar stations with missing precipitation data. Despite deliberately selecting events that maximize the likelihood of observing vertical differences in horizontal advection, no clear case emerges in which altitude-wide motion estimation provides a substantial advantage over traditional two-dimensional motion field estimation.

Taken together, these findings suggest that, for the dataset we used, vertical variability in horizontal precipitation motion is generally not prominent enough to be exploited by independent altitude-wise motion field estimation. This observation is consistent with the strong inter-altitude correlations reported in the previous section and further explains the limited quantitative gains observed for the volumetric approach.

Section V Summary

In terms of aggregate nowcasting performance, the volumetric approach does not reduce continuous error metrics relative to the 2D baseline and exhibits a small but systematic positive bias at longer lead times. On the other hand, categorical verification reveals a consistent improvement in Recall and Equitable Threat Score beyond approximately 30 minutes without a substantial loss in Precision. However, the increase in Recall is in a large part gained from non-physical cell-splitting artifacts that are caused by the design of our volumetric motion field estimator and evaluation on vertically pooled nowcasts.

The subsequent motion field correlation analysis revealed that inter-altitude motion field layers are strongly correlated across the dataset, including during convective summer months, suggesting that horizontal advection is generally vertically coherent. No situations with pronounced vertical variability in horizontal motion that would demonstrate clear qualitative advantages for altitude-wise motion estimation were identified in the whole dataset.

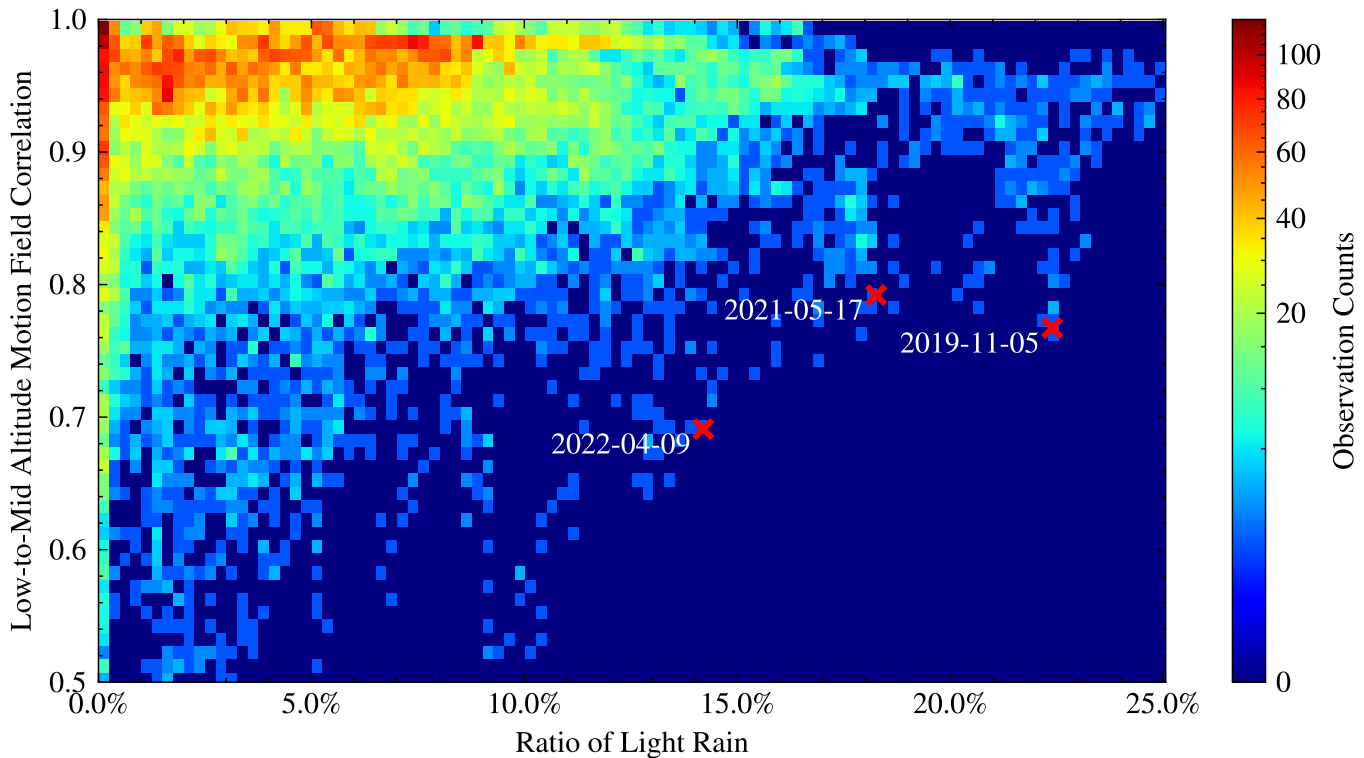


Fig. 15. Two-dimensional histogram of dataset samples as a function of precipitation coverage and inter-altitude motion field correlation. The horizontal axis shows the ratio of CMAX-pooled pixels exceeding 20 dBZ, while the vertical axis shows the Pearson correlation between horizontal motion fields estimated at the lowest altitude layer (500–1000 m above ground level) and a mid-level layer (2500–3000 m above ground level). Red hues indicate the highest density of samples, dark blue no such samples. The three crosses denote events selected for qualitative evaluation.

VI. CONCLUSION

In this paper, we proposed a 3D Motion Field U-Net that estimates altitude-wise horizontal advection of precipitation from sequences of volumetric radar observations. The central hypothesis was that altitude-wise motion field estimation would improve extrapolation-based precipitation nowcasting, particularly during the warm season when convective storms are expected to introduce stronger vertical variability in precipitation dynamics.

To test this hypothesis, we compared the proposed volumetric model against a baseline model of identical architecture operating on vertically pooled 2D radar composites. This controlled experiment ensured that any observed performance differences could be attributed solely to the use of volumetric information. The evaluation revealed mixed results: while the volumetric model underperformed the 2D baseline in continuous error metrics, it consistently improved categorical scores, most notably Recall, at longer lead times. However, qualitative analysis demonstrated that these gains largely stem from non-physical cell-splitting artifacts introduced by independently estimated motion fields at different altitude levels, rather than from more accurate representation of storm evolution.

An advantage of the proposed framework is its computational efficiency. The GPU-accelerated nature and custom batch processing of the 3D Motion Field U-Net enabled large-scale analysis of the estimated volumetric motion fields across the entire dataset from the Slovak radar network. This allowed

us to go beyond standard nowcasting verification and examine the structure of the estimated motion fields. The analysis revealed strong inter-altitude correlations throughout the radar volume, with only a gradual decrease in similarity at larger vertical separations and in the sparsely observed upper levels. Importantly, the dominant direction of horizontal advection remained highly consistent across altitudes.

Contrary to our initial expectations, the strongest inter-altitude correlations were observed during the warm season, despite the higher prevalence of deep convective storms. Even when focusing on carefully selected events characterized by both extensive precipitation coverage and unusually low inter-altitude correlation, the estimated motion fields at different heights remained largely aligned. These findings indicate that, for the dataset considered, vertical variability in horizontal precipitation motion is generally low and insufficient to give the proposed model a systematic advantage over traditional two-dimensional motion field estimation.

Several limitations should be considered when interpreting these results. First, the analysis is based on a single national radar network and a relatively limited timespan. Second, the proposed framework assumes pure Lagrangian persistence and does not explicitly model growth, decay, or any other evolution of precipitation besides horizontal advection, potentially limiting the ability to disentangle true vertical motion differences from intensity evolution effects. Finally, motion fields at different altitude levels are estimated independently, without explicit physical constraints enforcing vertical consistency. This design

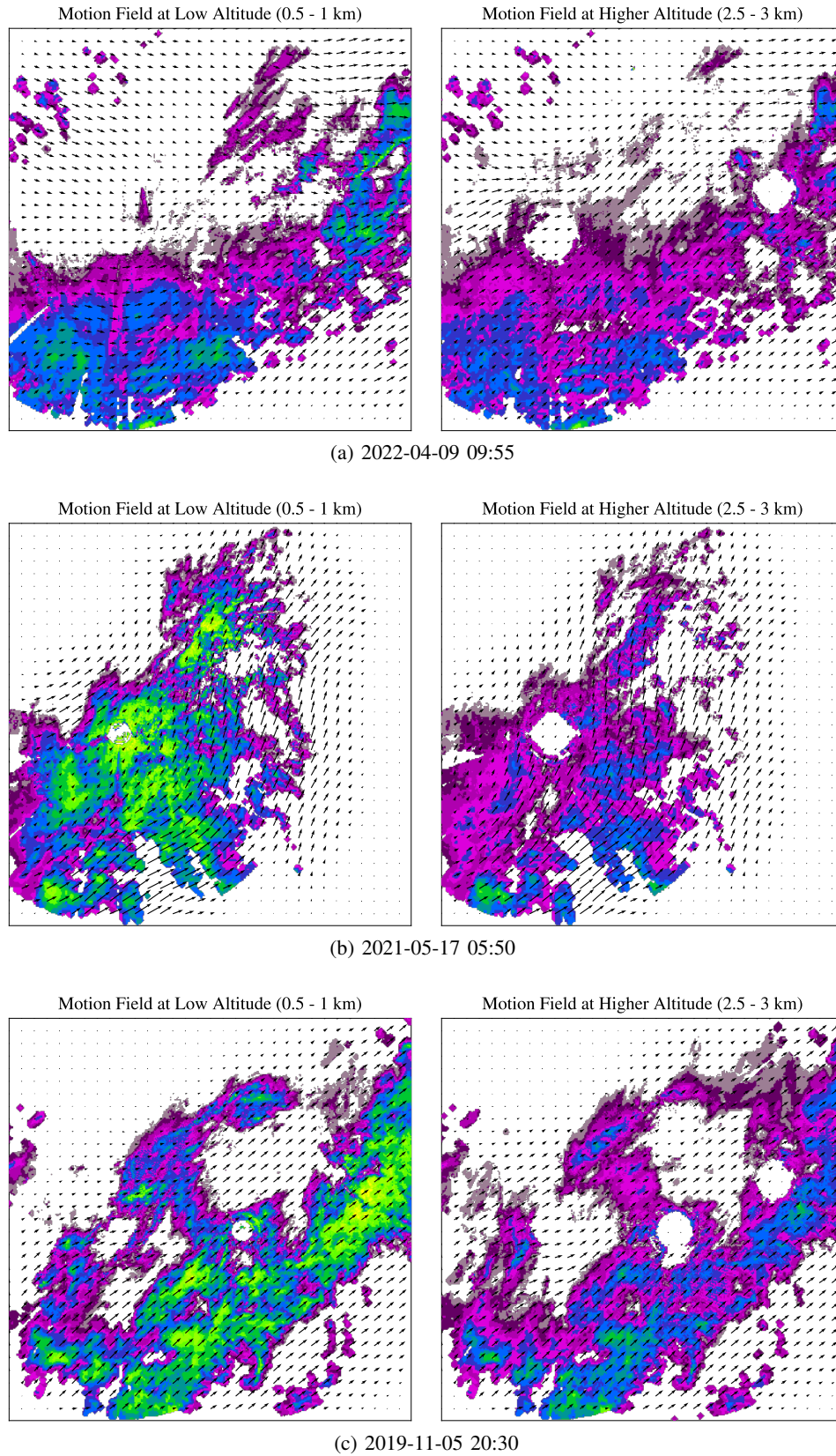


Fig. 16. Estimated horizontal motion fields and corresponding precipitation fields at the lowest altitude layer (500–1000 m above ground level; left) and a mid-level layer (2500–3000 m above ground level; right) for three events selected for their low inter-altitude motion correlation and high precipitation coverage. The animated figures are available online at: <https://pavlikp.github.io/3DMF/#figure-16>

choice contributes to the observed cell-splitting artifacts. We suggest that future work should employ vertically coupled or physically regularized estimators.

In conclusion, our results suggest that the Slovak radar dataset does not contain precipitation events in which independent altitude-wise motion field estimation yields a clear benefit for extrapolation nowcasting. While this does not imply that volumetric motion fields are universally uninformative as previous studies have demonstrated their utility in other climatic regimes, it does indicate that such situations are rare under the conditions examined in this study. However, other datasets from regions with more frequent and intense vertical wind shear and less vertical consistency during storms may be able to fully exploit the potential of volumetric motion estimation.

More broadly, this study highlights the importance of critically assessing the practical value of three-dimensional data representations in AI-based precipitation nowcasting and meteorology in general. In scenarios where vertical coherence of horizontal motion is prevalent, the increased memory and computational cost of volumetric models may not be justified by marginal performance gains.

ACKNOWLEDGMENTS

This work was partially funded by the European Union, under the project LorAI - Low Resource Artificial Intelligence, GA No. 101136646 and by V4Grid, an Interreg Central Europe Programme project co-funded by the European Union, project No. CE0200803. The research was performed in cooperation with Softec, Ltd. and Slovak Hydrometeorological Institute.

Research results were obtained using the computational resources procured in the national project National competence centre for high performance computing (project code: 311070AKF2) funded by European Regional Development Fund, EU Structural Funds Informatization of society, Operational Program Integrated Infrastructure.

CODE AVAILABILITY

The source code for all the models used in the experiments, along with the training, evaluation and visualization scripts and a link to download the used dataset are available at: <https://github.com/kinit-sk/volumetric-motion-fields>

REFERENCES

- [1] WMO, *Guidelines for Nowcasting Techniques*. 7 bis, avenue de la Paix, P.O. Box 2300, CH-1211 Geneva 2, Switzerland: World Meteorological Organization, 2017, no. 978-92-63-11198-2.
- [2] W. Zhang, T. Zhou, and P. Wu, "Anthropogenic amplification of precipitation variability over the past century," *Science*, vol. 385, no. 6707, pp. 427–432, 2024. [Online]. Available: <https://www.science.org/doi/abs/10.1126/science.adp0212>
- [3] P. Novák, L. Březková, and P. Frolík, "Quantitative precipitation forecast using radar echo extrapolation," *Atmospheric Research*, vol. 93, no. 1, pp. 328–334, 2009, 4th European Conference on Severe Storms. [Online]. Available: <https://www.sciencedirect.com/science/article/pii/S0169809508003025>
- [4] A. W. Seed, "A dynamic and spatial scaling approach to advection forecasting," *Journal of Applied Meteorology*, vol. 42, no. 3, pp. 381 – 388, 2003. [Online]. Available: https://journals.ametsoc.org/view/journals/apme/42/3/1520-0450_2003_042_0381_adassa_2.0.co_2.xml
- [5] N. E. Bowler, C. E. Pierce, and A. W. Seed, "Steps: A probabilistic precipitation forecasting scheme which merges an extrapolation nowcast with downscaled nwp," *Quarterly Journal of the Royal Meteorological Society: A journal of the atmospheric sciences, applied meteorology and physical oceanography*, vol. 132, no. 620, pp. 2127–2155, 2006.
- [6] S. Pulkkinen, V. Chandrasekar, and T. Niemi, "Lagrangian integro-difference equation model for precipitation nowcasting," *Journal of Atmospheric and Oceanic Technology*, vol. 38, no. 12, pp. 2125–2145, 2021.
- [7] S. Pulkkinen, V. Chandrasekar, A. von Lerber, and A.-M. Harri, "Nowcasting of convective rainfall using volumetric radar observations," *IEEE Transactions on Geoscience and Remote Sensing*, vol. 58, no. 11, pp. 7845–7859, 2020.
- [8] X. Shi, Z. Chen, H. Wang, D.-Y. Yeung, W.-K. Wong, and W.-c. Woo, "Convolutional lstm network: A machine learning approach for precipitation nowcasting," *Advances in neural information processing systems*, vol. 28, 2015.
- [9] Y. Wang, M. Long, J. Wang, Z. Gao, and P. S. Yu, "Predrnn: Recurrent neural networks for predictive learning using spatiotemporal lstms," *Advances in neural information processing systems*, vol. 30, 2017.
- [10] G. Ayzel, T. Scheffer, and M. Heistermann, "Rainnet v1. 0: a convolutional neural network for radar-based precipitation nowcasting," *Geoscientific Model Development*, vol. 13, no. 6, pp. 2631–2644, 2020.
- [11] C. Keil and G. C. Craig, "A displacement and amplitude score employing an optical flow technique," *Weather and Forecasting*, vol. 24, no. 5, pp. 1297 – 1308, 2009. [Online]. Available: https://journals.ametsoc.org/view/journals/wefo/24/5/2009waf2222247_1.xml
- [12] X. Shi, Z. Gao, L. Lausen, H. Wang, D.-Y. Yeung, W.-k. Wong, and W.-c. Woo, "Deep learning for precipitation nowcasting: A benchmark and a new model," *Advances in neural information processing systems*, vol. 30, 2017.
- [13] S. Ravuri, K. Lenc, M. Willson, D. Kangin, R. Lam, P. Mirowski, M. Fitzsimons, M. Athanassiadou, S. Kashem, S. Madge *et al.*, "Skilful precipitation nowcasting using deep generative models of radar," *Nature*, vol. 597, no. 7878, pp. 672–677, 2021.
- [14] Y. Zhang, M. Long, K. Chen, L. Xing, R. Jin, M. I. Jordan, and J. Wang, "Skilful nowcasting of extreme precipitation with nowcastnet," *Nature*, vol. 619, no. 7970, pp. 526–532, 2023.
- [15] J. Ritvanen, B. Harnist, M. Aldana, T. Mäkinen, and S. Pulkkinen, "Advection-free convolutional neural network for convective rainfall nowcasting," *IEEE Journal of Selected Topics in Applied Earth Observations and Remote Sensing*, vol. 16, pp. 1654–1667, 2023.
- [16] P. Pavlík, M. Východ, A. B. Ezzeddine, and V. Rozinajová, "Fully differentiable lagrangian convolutional neural network for physics-informed precipitation nowcasting," *Applied Computing and Geosciences*, p. 100296, 2025.
- [17] D.-K. Kim, T. Suezawa, T. Mega, H. Kikuchi, E. Yoshikawa, P. Baron, and T. Ushio, "Improving precipitation nowcasting using a three-dimensional convolutional neural network model from multi parameter phased array weather radar observations," *Atmospheric Research*, vol. 262, p. 105774, 2021. [Online]. Available: <https://www.sciencedirect.com/science/article/pii/S0169809521003306>
- [18] P. Pavlík, V. Rozinajová, and A. B. Ezzeddine, "Radar-based volumetric precipitation nowcasting: A 3d convolutional neural network with u-net architecture." in *CDCEO@IJCAI*, 2022, pp. 65–72.
- [19] N. Sun, Z. Zhou, Q. Li, and J. Jing, "Three-dimensional gridded radar echo extrapolation for convective storm nowcasting based on 3d-convlstm model," *Remote Sensing*, vol. 14, no. 17, p. 4256, 2022.
- [20] K.-S. Chung, Y.-C. Hsu, Y.-H. Tsou, and H.-H. Lin, "Investigating the spatiotemporal characteristics of motion fields using three-dimensional radar echoes to construct an ensemble nowcasting system," *Quarterly Journal of the Royal Meteorological Society*, vol. 151, no. 768, p. e4935, 2025.
- [21] H. Chen, W. Han, H. Sun, N. Lin, X. Song, Y. Yang, J. Tian, Y. Liu, J.-R. Wen, X. Zhang *et al.*, "Nowcast3d: Reliable precipitation nowcasting via gray-box learning," *arXiv preprint arXiv:2511.04659*, 2025.
- [22] B. D. Lucas and T. Kanade, "An iterative image registration technique with an application to stereo vision," in *IJCAI'81: 7th international joint conference on Artificial intelligence*, vol. 2, 1981, pp. 674–679.
- [23] J. Vido, P. Borsányi, P. Nalevanková, M. Hanzelová, J. Kučera, and J. Škvarenina, "Thunderstorm climatology of slovakia between 1984–2023," *Theoretical and Applied Climatology*, vol. 155, no. 9, pp. 8651–8679, 2024.
- [24] D. Li, Y. Qi, and H. Li, "Statistical characteristics of convective and stratiform precipitation during the rainy season over south china based on gpm-dpr observations," *Atmospheric Research*, vol. 301, p. 107267, 2024.

- [25] J. S. Marshall and W. M. K. Palmer, "The distribution of raindrops with size," *Journal of the Atmospheric Sciences*, vol. 5, no. 4, pp. 165–166, 1948. [Online]. Available: [https://doi.org/10.1175/1520-0469\(1948\)005<0165:TDORWS>2.0.CO;2](https://doi.org/10.1175/1520-0469(1948)005<0165:TDORWS>2.0.CO;2)
- [26] T. Nagasato, K. Ishida, A. Ercan, T. Tu, M. Kiyama, M. Amagasaki, and K. Yokoo, "Extension of convolutional neural network along temporal and vertical directions for precipitation downscaling," *arXiv preprint arXiv:2112.06571*, 2021.
- [27] Y. Ye, F. Gao, W. Cheng, C. Liu, and S. Zhang, "Msstnet: A multi-scale spatiotemporal prediction neural network for precipitation nowcasting," *Remote Sensing*, vol. 15, no. 1, p. 137, 2022.
- [28] P. Pavlík, M. Schleiss, A. B. Ezzeddine, and V. Rozinajová, "Do echo top heights improve deep learning rainfall nowcasts? a case study in the netherlands," in *Transactions on Large-Scale Data-and Knowledge-Centered Systems LVIII*. Springer, 2025, pp. 66–92.